Effect of the Intrinsic Pinning on Transport Critical Currents and Two-Dimensionality of Vortex Motion in High Temperature Superconducting Oxides

西嵜, 照和
九州大学理学研究科物理学専攻

https://doi.org/10.11501/3075394

出版情報：九州大学, 1993, 博士（理学）, 課程博士
バージョン：
権利関係：

Effect of the Intrinsic Pinning on Transport Critical Currents and Two-Dimensionality of Vortex Motion in High Temperature Superconducting Oxides

西　嵜　照　和

Effect of the Intrinsic Pinning on Transport Critical Currents and Two - Dimensionality of Vortex Motion in High Temperature Superconducting Oxides

酸化物高温超伝導体の輸送臨界電流に対する
固有ピン止めの効果と磁束運動の二次元性

Terukazu NISHIZAKI
西嵜照和

Department of Physics, Faculty of Science
Kyushu University
1994

Preface

The study has been performed under the guidance of Professor Takafumi Aomine and Professor Takeshi Fukami during 1991-1993 at Kyushu University. The present thesis is concerned with transport critical currents and flux pinning properties in high T_c superconductors (HTSC's). Efforts were mainly made to understand the following matters; (a) Intrinsic pinning properties due to the spatial variation of the order parameter along the c axis. (b) The effect of the macroscopic driving force on the critical current in the mixed state for HTSC's with different degrees of two-dimensionality. (c) The anisotropic natures in the mixed state related to their layered crystal structure and the short coherence length. Systematic studies about the transport critical current density J_c are carried out using epitaxial thin films of $YBa_2Cu_3O_{7-\delta}$ (YBCO) and $Nd_{2-x}Ce_xCuO_{4-\delta}$ (NCCO) as a function of magnetic field B, its direction and temperature in a wide range. The subjects (a), (b) and (c) mentioned above are closely related to the degree of the two-dimensionality, which is different from one material to another and depends on temperatures. Therefore, the vortex state and the magnetic field-direction dependence of $J_c(B)$ would vary with a variety of HTSC and with temperatures. Since it is important for the study of the mixed state to consider the degree of two-dimensionality of the materials, the results obtained are compared with those of other HTSC's such as $Bi_2Sr_2CaCu_2O_{8+y}$, $YBa_2Cu_3O_{7-\delta}$ /$PrBa_2Cu_3O_{7-\delta}$ (YBCO/PBCO) multilayer thin films etc. with the different two-dimensionality . Furthermore, the flux pinning mechanisms and the origin of the angular dependences of J_c for each material are discussed.

The author is most grateful to Professor Takafumi Aomine for valuable advice, discussions throughout the course of this work and critical reading of the manuscript. The author also wishes to thank Professor Takeshi Fukami for his helpful suggestions and critical reading of the manuscript.

The author is grateful to Professor Masashi Tachiki of Tohoku University for valuable discussions about intrinsic pinning mechanisms.

The present thesis is based upon collaboration with Institute for Chemical Research of Kyoto University, Ube Laboratory of Ube Industries Limited and NTT Interdisciplinary Laboratories of Nippon Telegraph and Telephone Corporation. The author is grateful to Professor Yoshichika Bando and Dr. Takahito Terashima of Kyoto University and Drs. Itsuhiro Fujii, Kazunuki Yamamoto and Shizuka Yoshii of Ube Industries for suppling YBCO epitaxial thin films. The author is also grateful to Drs. Shugo Kubo and Minoru Suzuki of NTT for suppling NCCO epitaxial thin films and for their valuable discussions.

The author is indebted to the following people for providing the YBCO/PBCO multilayer thin films which are used for comparison in Fig.6.19 of chapter 6 : Professor B. R. Zhao, Dr. X. G. Qiu and Professor L. Lin of National Laboratory for Superconductivity, Institute of Physics, Chinese Academy of Science.

The author would like to thank the staffs, Messrs. Tatsuo Aizawa, Tsutomu Soejima, Toshihiro Hotta and Hirotaka Ueda, of the Laboratory of Low Temperature Physics of Kyushu University for operation of a magnet and for use of liquid helium.

Finally, the author is greatly indebted to Mr. Fusao Ichikawa and many other members of Aomine laboratory for their kind discussions and assistance.

November 1993

Terukazu Nishizaki

Contents

List of Figures

List of Tables

Chapter 1

Introduction

1.1 History and introductory remarks

In 1986 Bednortz and Müller discovered a high T_c superconductor (HTSC) $La_{1-x}Ba_x$ CuO_4 with transition temperatures T_c about 30 K; that was reported by a paper entitled "Possible High T_c Superconductivity in the Ba-La-Cu-O System"[1]. Many researchers all over the world took an active interest in searching HTSC, and the highest achieved transition temperature began a rapid rise. By the beginning of 1987, $La_{2-x}Sr_xCuO_4$ system was reported by several groups[2–4], and it had T_c close to 40 K and up to 52 K under high pressures[5]. Soon later, $YBa_2Cu_3O_{7-\delta}$ with T_c of 90 – 95 K was discovered[6,7], and T_c is above the liquid nitrogen temperature. The discovery of this material has led to many speculations about superconducting applications at liquid nitrogen temperature (T = 77.3 K). After one year, Bi-Sr-Ca-Cu-O[8–10] and Tℓ-Ba-Ca-Cu-O[11–14] systems were discovered and T_c of these new oxides achieved the value of T_c = 110 – 120 K. These oxides show superconductivity by introducing free holes by doping other elements with excess charge. An electron-doped copper oxide superconductor, $Ln_{2-x}Ce_xCuO_{4-y}$ system (Ln = Nd, Sm, Pr) with T_c up to 24 K for x = 0.15, was discovered[15,16]. In 1993 new Hg-Ba-Ca-Cu-O system was discovered and at present T_c reaches 130 – 150 K[17,18].

These high T_c superconductors are characterized not only by their high transition temperatures but also by (a) quasi two-dimensional (2D) anisotropy due to

their layered crystal structures and (b) extreme type II superconducting behavior [Ginzburg-Landau (G-L) parameter $\kappa \gg 1$] due to a short coherence length and a long penetration depth. In particular, in the case of $YBa_2Cu_3O_{7-\delta}$, for example, the coherence length along the c axis ξ_c ($\sim$ 2 Å at 0 K) ia small in comparison with the lattice constant (c = 11.7 Å). The physical quantities in the magnetic field B depend on the magnitude and direction of the magnetic field because of the large anisotropy. For example, it is expected that the resistivity and the critical current for $B \parallel c$ is different from those for $B \parallel ab$. This difference is closely related to the angular dependence of the upper critical field B_{c2} and to the anisotropic pinning mechanism. Since a degree of the anisotropy is different from one material to another, the vortex state and the angular dependence of $J_c(B)$ would vary in a variety of HTSC. Recently, a new vortex state so called 2D pancake vortex state[19] was suggested for highly two-dimensional layered systems; this state is different from the Abrikosov vortex state. Therefore, it is important for a study of the mixed state to consider the degree of anisotropy of the material, and to clearly define the configuration of magnetic field, the transport current and the crystal axes.

As for flux pinning mechanisms in HTSC, various pinning centers such as twin planes, precipitates, grain boundaries, etc. have been considered. At present, however, thin films of high quality and epitaxial thin films have large J_c of the order of 10^6 A/cm^2 at 77 K in the case of YBCO. J_c of sintered bulk samples and polycrystalline thin films is smaller than that of epitaxial ones. Such tendency is completely contrary to conventional type II superconductors. Thus it is a big problem what becomes strong pinning centers in high J_c epitaxial thin films of HTSC. Recently, for the strong pinning force epitaxial thin films with good quality an intrinsic pinning mechanism was proposed[20–23]. The intrinsic pinning mechanism is based on a spatial variation of the order parameter along the c direction due to the layered crystal structure and the short ξ_c, so a strong pinning force is expected even in single-crystalline samples. Furthermore, the model predicts the magnetic field-direction

dependence of $J_c(B)$[24]. Therefore the intrinsic pinning mechanism would be one of the most important pinning mechanisms to consider the mixed state in HTSC.

1.2 Crystal structures of HTSC

The crystal structures of $YBa_2Cu_3O_{7-\delta}$ (YBCO), $Nd_{2-x}Ce_xCuO_{4-\delta}$ (NCCO) and $Bi_2Sr_2CaCu_2O_{8+y}$ (Bi2212) are shown in Fig.1.1. For clarify, oxygen atoms at the intersection of two lines are omitted in the cases of YBCO and Bi2212. YBCO has an orthorhombic structure, while NCCO and Bi2212 have tetragonal structures. The lattice parameters of YBCO[25], NCCO[26] and Bi2212[27] are shown in Table 1.1. These HTSC's have layered structures, and include one or several CuO_2 conducting planes in the unit cell. In many cases, the CuO_2 square lattice containes one oxygen atom at the center of the Cu-Cu bond.

In the case of YBCO with $\delta = 0$, all the oxygen sites along the a direction of the basal plane are empty, and all of those along the b direction occupied. Thus Cu-O chains appear along the b direction. The missing oxygens cause coppers to move slightly closer together along the a direction, therefor inducing the orthombic distortion with $a < b$. There is a distance of 3.18 Å between the CuO_2 double layers which separated by the yttrium. CuO_2 planes are coupled to CuO chains with the distance of 4.25 Å through apical oxygen atoms in the BaO planes.

NCCO is a Ce^{4+} doped material with the formula $Nd_{2-x}Ce_xCuO_{4-\delta}$. This material has basically the Nd_2CuO_4 (T′-phase) structure, which consists of CuO_2 seats. This structure has no apical oxygen above and below the CuO_2 plane in contrast to the T-phase structure with Cu-O octahedra, as observed in $La_{2-x}Sr_xCuO_4$. NCCO shows a maximum T_c ($\sim$ 24 K) at $x = 0.15$, and the value of T_c changes sensitively with Ce concentration.

In the case of Bi2212, the conducting plane which consists of CuO_2 double layers separated by non-conducting BiO double layers. The calcium atoms exist between

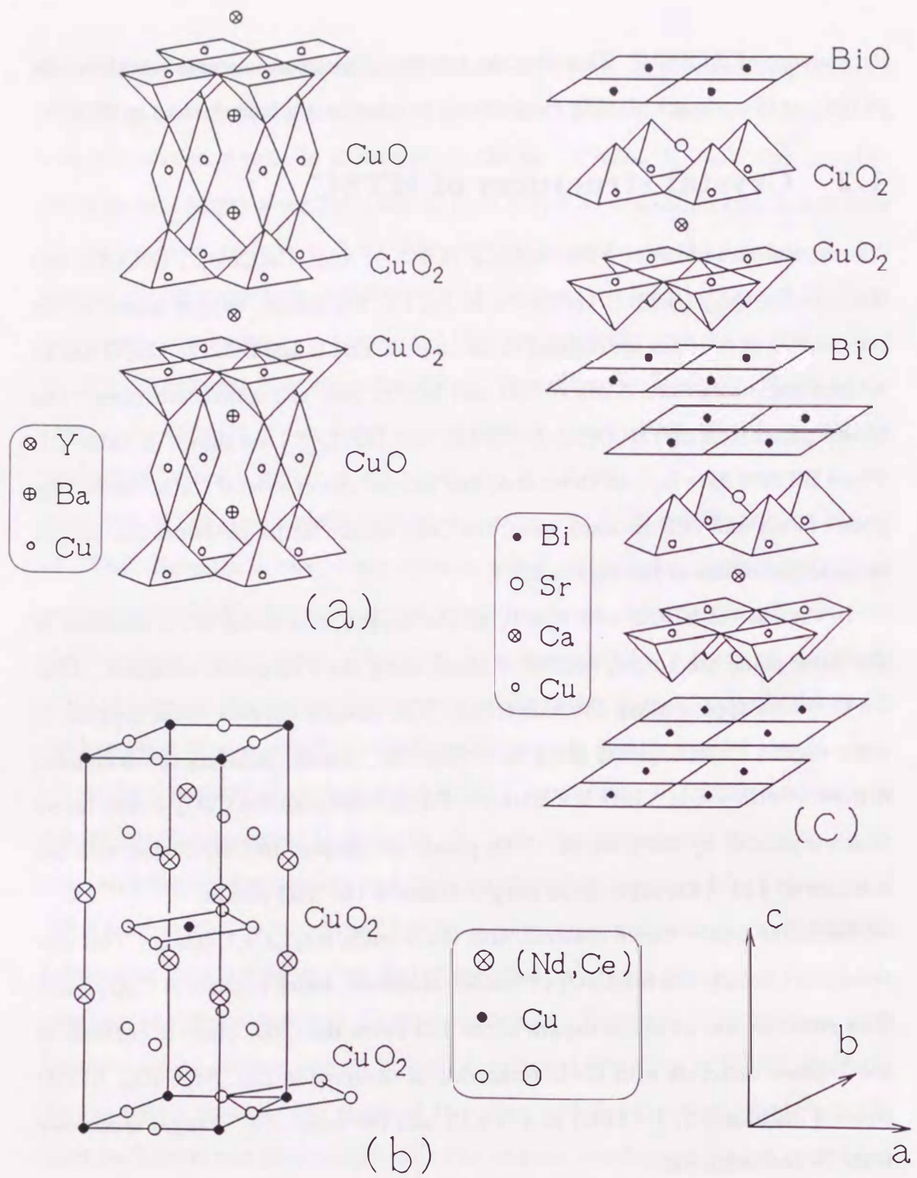

Fig. 1.1. The crystal structures of (a) $YBa_2Cu_3O_{7-\delta}$, (b) $Nd_{2-x}Ce_xCuO_{4-\delta}$ and (c) $Bi_2Sr_2CaCu_2O_{8+y}$. In order to simplify the figure, oxygen atoms which exit at a point of intersection of each two lines are omitted in case of YBCO and Bi2212.

Table 1.1. Lattice parameters of YBCO, NCCO and Bi2212.

	YBCO	NCCO	Bi2212
a (Å)	3.82	3.95	5.40
b (Å)	3.89	3.95	5.40
c (Å)	11.70	12.07	30.65

the CuO_2 planes with apical oxygens. Bi2212 is the case with $n = 2$ in the form of $Bi_2Sr_2Ca_{n-1}Cu_nO_{2n+6}$ ($n = 1, 2$ and 3) family with T_c 's of 20, 85 and 110K, respectively.

Anisotropic superconducting properties due to these layered crystal structures will be described in the chapter 2.

1.3 Flux pinning experiments

1.3.1 Flux pinning and the critical state

As first predicted by Abrikosov[28], when the external magnetic fields beyond the lower critical field B_{c1} is applied to a type II superconductor, the field penetrates into the superconductor in the form of flux lines (vortices), each of which carries single flux quantum ϕ_0:

$$\phi_0 = \frac{h}{2e} = 2.07 \times 10^{-7} \quad (\mathrm{G\ cm^2}) , \tag{1.1}$$

$$= 2.07 \times 10^{-15} \quad (\mathrm{T\ m^2}) , \tag{1.2}$$

where h is the Planck's constant and e the electron charge. Type II superconductors are characterized by $\kappa > 1/\sqrt{2}$. The criterion of $\kappa = 1/\sqrt{2}$ separating type I and type II superconductors is determined as a value at which the cancellation of the positive and negative contribution to the wall energy occurs[29]. Usually, flux lines are arranged in the form of a triangular flux-line lattice and these distribution is referred to as the mixed state.

When there is a transport current with a density J in the mixed state of superconductors, flux lines experience the Lorentz force F_L, given by

$$\boldsymbol{F}_L^{(l)} = \boldsymbol{J} \times \boldsymbol{\phi}_0 \qquad \text{per unit length of flux line,} \tag{1.3}$$

$$\boldsymbol{F}_L^{(v)} = \boldsymbol{J} \times \boldsymbol{B} \qquad \text{per unit volume of superconductor,} \tag{1.4}$$

due to an electromagnetic dynamical effect. Here $\boldsymbol{\phi}_0$ is a vector, and $\boldsymbol{B}$ the flux density ($= n\boldsymbol{\phi}_0$, where n is the number of flux lines per unit area). Flux lines interact with inhomogenities in the sample such as grain boundaries, dislocations and precipitates. The force per unit volume which the flux lines receive from inhomogenities is called a volume pinning force (or a pinning force density) F_p and such kind of inhomogenities are called the pinning centers. The movement of flux lines occurs when the driving force F_L exceeds F_p. The critical current density J_c is defined as J at which F_L is just balanced by F_p:

$$\boldsymbol{J}_c \times \boldsymbol{\phi}_0 = -\boldsymbol{F}_p^{(l)} \qquad \text{per unit length of flux line,} \tag{1.5}$$

$$\boldsymbol{J}_c \times \boldsymbol{B} = -\boldsymbol{F}_p^{(v)} \qquad \text{per unit volume of superconductor.} \tag{1.6}$$

If flux lines move in response to the driving force with a velocity v, the energy of the current is dissipated in superconductors. According to Faraday's law, moving flux lines induce an electric field,

$$\boldsymbol{E} = n\boldsymbol{\phi}_0 \times \boldsymbol{v} = \boldsymbol{B} \times \boldsymbol{v} \quad , \tag{1.7}$$

which is oriented parallel to $\boldsymbol{J}$, so the superconductor becomes resistive.

The critical state is defined as a state that the critical current folows everywhere in the superconductor. This state requires that an equilibrium between the driving force and the pinning force realizes everywhere in the superconductors, namely any driving force is just opposed by the pinning force. Any disturbance by changing either the transport current or the external magnetic field results in a redistribution of the flux until the critical state is restored. The total current density (*i.e.* the

sum of magnetization and transport current densities) $\boldsymbol{J} = \boldsymbol{\nabla} \times \boldsymbol{H}$ and the driving force is equivalent to the Lorentz force $\boldsymbol{J} \times \boldsymbol{\phi}_0$. The critical state equation can be written

$$\boldsymbol{J}_c \times \boldsymbol{\phi}_0 = -\boldsymbol{F}_p^{(l)}(B) = \boldsymbol{\nabla} \times \boldsymbol{H}(B) \times \boldsymbol{\phi}_0 \quad , \tag{1.8}$$

$$\boldsymbol{J}_c \times \boldsymbol{B} = -\boldsymbol{F}_p^{(v)}(B) = \boldsymbol{\nabla} \times \boldsymbol{H}(B) \times \boldsymbol{B} \quad , \tag{1.9}$$

where the F_p is now recognized to be a function of the local value of B. The resulting flux distribution is derived from

$$|\boldsymbol{\nabla} \times \boldsymbol{H}(B)| = \left| \frac{\partial H}{\partial B} \boldsymbol{\nabla} \times \boldsymbol{B} \right| = J_c(B) = \frac{F_p^{(v)}}{B} \quad , \tag{1.10}$$

where $\boldsymbol{H}(B)$ is the external field that would be in equilibrium with the internal induction B, and $\partial H/\partial B$ is the slope of the ideal reversible magnetization curve for the material.

The flux distribution within the superconductor can be determined if it is known how either J_c or F_p varies with B. Bean[30] and London[31] made the first attempt to solve the critical state assuming that J_c was constant, independent of B; in this case $F_p \propto B$. In the Kim model[32], on the other hand, F_p has been assumed to be independent of B, and the critical current density is given by

$$J_c = \frac{A}{B + B_0} \quad , \tag{1.11}$$

where A and B_0 are empirical constants. The same $1/B$ dependence of J_c has also been reported by Campbell *et al.*[33], Anderson[34], Silcox and Rollins[35] and Friedel[36].

Other critical state models have been suggested by many authors. Fietz *et al.*[37] related a critical current to magnetization curves using an exponential dependence of J_c on B. Other forms used are: $J_c \propto B^{-1/2}$ (Yasukouchi *et al.*[38]), $J_c \propto (B_{c2} - B)$ (Goedemoed *et al.*[39]) and $J_c \propto B^{-1/2}(B_{c2} - B)$ (Alden and Livingston[40], Campbell *et al.*[41] and Coffey[42]). Irie and Yamafuji[43] make a simple assumption of $J_c \propto B^{-\gamma}$, where γ is a constant of any value.

In addition, Fietz and Webb[44], and Hampshire and Taylor[45] have shown that $J_c \propto [B_{c2}(T)]^m f(b) = [B_{c2}(T)]^m b^p (1-b)$ is valid over the range $0.3 \leq b \leq 1$, where b is defined by B/B_{c2}. The constants m and p depend on pinning mechanisms. In this form, the temperature dependence of J_c results from the temperature dependence of B_{c2}. When $J_c b$ is plotted against b at a constant temperature, this curve has a maximum at a special value of b. The maximum appears at the same b for any T as long as m and p are not dependent on T, though the maximum decreases with increasing T. Therefore, this equation is powerful to analyze the experimental data and to discuss the pinning mechanisms.

In order to obtain the information about the vortex pinning, the critical current density and the vortex state, a great variety of experimental techniques are available. Here, several experimental techniques and their characteristics are described.

1.3.2 Transport measurements

From the experimental point of view, measuring the transport critical current is the most simplest method to determine the pinning force, because this method does not depend on any theoretical model. However, this method must be used only for samples with small cross sections where the flux density and pinning force density do not vary. From I-V curves observed, the critical current I_c is usually determined on the basis of a voltage-over-distance criterion, *e.g.*, 1 μV/cm. If the superconductor is in the mixed state, the volume pinning force as a function of B is simply given by

$$F_p = J_c \times B = \frac{I_c}{S} B \quad , \tag{1.12}$$

where S is a cross section of the sample.

Much more information can be obtained from I-V characteristics. For example, it is important for the study of the vortex glass transition to obtain informations whether I-V curves show ohmic, the flux flow resistance or a power-law dependence. Furthermore, the pinning force as a function of the applied field direction can be

obtained easily. Because the direction of the magnetic field determines the shape of vortices and their direction in the crystal, and the direction of the transport current determines the Lorentz force (driving force). Hence, the pinning force direction varies in response to the driving force direction. On the other hand, J_c estimated from DC or AC magnetization method which will be described below depends on the theoretical model. Furthermore, since J_c is composed of two components it is difficult to separate it into two components due to highly anisotropy of HTSC.

In this thesis the transport method was used for thin film samples of HTSC with a small cross sections. The details of the measurement system will be described in section 3.3.

1.3.3 Magnetization measurement

Transport critical current measurements are impractical for samples with large cross sections due to the heating problem at the joints of contact between superconductors and current reads. Because I_c is around 2000 A for a 1 mm diamater-superconducting wire with $J_c = 3 \times 10^5$ A/cm^2. This problem can be avoided in magnetization measurements, where the transport current is replaced by induced circular currents. The relation between the magnetization and the critical current is established using the concept of the critical state introduced by Bean[30]. Moreover, some extensions can be made, *e.g.*, the B dependence of J_c giving rise to a positional dependence, using a Taylor expansion[44].

At present, the magnetization M is usually obtained by means of a superconducting quantum interface device (SQUID) or a vibrating sample magnetometer (VSM). All magnetization techniques make use of the induced voltage which appears by a flux change in a pick-up coil surrounding the sample. Since the flux change in a sample is equal to the time integral of the induced voltage, in general, the magnetization measurement only gives the quantity $F_p(B)$ in the form of an integral. Usually for the analysis of experimental results a reasonable function form

$F_p(B)$ is assumed with some adjustable parameters.

If the hysteresis of the magnetization curve is small, the situation is greatly simplified. In this case the relative difference between the maximum and minimum flux density in the sample is also small and the pinning force density is assumed to be constant across the sample. For a cylindrical sample this leads to critical current density[44]

$$J_c^M = 15\frac{M^+ - M^-}{R} = 15\frac{\Delta M}{R} \quad , \tag{1.13}$$

in which the sample radius R is given in cm, J_c^M in A/cm^2 and M in emu/cm^3. Here M^+ and M^- are the magnetization values in increasing and decreasing fields, respectively.

1.3.4 AC technique

The advantages of measuring the response of a type II superconductor to an AC ripple were realized by Bean[46]. The principle of this method is to superpose a small AC magnetic field component h_0 on a longitudinal DC magnetic field. An information on the flux density profile inside the superconductor can be derived from the voltage induced in a pick-up coil around the sample, using the various ways such as a harmonic analysis, a direct waveform analysis and an integration analysis of the complete waveform using a lock-in amplifier. The last technique is called Campbell's method. In case of the Campbell's method, the magnetic flux Φ going in and out of the sample was measured as a function of the ac field h_0, and the penetration depth λ' of the AC field was derived as[47]

$$\lambda' = \frac{1}{2w}\frac{\partial \Phi}{\partial h_0} \quad , \tag{1.14}$$

where w is the width of the sample. Plotting λ' vs. h_0, a linear relation is obtained in ordinary bulk superconductors. The slope of the linear line gives $1/\mu_0 J_c$, where μ_0 is the permeability of the vacuum.

The AC technique is the most powerful method to investigate granular samples of

HTSC. For example, the two sorts of critical current densities such as the intragrain critical current density and the intergrain one can be obtained separately[48,49]. It is difficult to separate the two components by using the other methods, because J_c^M obtained by the magnetization measurement is a mixture of two components of both inter- and intragrain critical current densities, on the contrary, the transport critical current density is mainly determined by weak links at intra- or intergrain parts.

1.3.5 Hall probe method

Kim *et al.* showed the Hall probe technique for the study of pinning force in superconductors[50]. For the wall thickness Δr of a superconducting tube is sufficiently small, one may assume that the flux density gradient within the material is constant. In this case the pinning force density is given by

$$F_p = J_c B = \pm B_m \frac{H - H_i}{\Delta r} \tag{1.15}$$

where $\pm$ signs stand for a increasing and decreasing the external magnetic field H, B_m is the mean flux density and H_i the field inside the hollow tube. Usually, H_i is measured by a small Hall probe.

1.3.6 Decoration technique

Decoration with magnetic particles has been shown to be a very powerful technique to investigate a flux line state. The first direct observation of the flux line lattice in type II superconductors has been achieved by Träuble and Essmann[51] using the decoration method. This method is based on the diffusion of evaporated small particles in the inhomogeneous magnetic field which generates a strong force, and particles at the sample surface were separated from each other.

For YBCO it has been reported that flux lines are pinned by twin planes, but other defects also contribute to the flux line disorder[52,53]. Moreover, it has been also demonstrated that the structure of the flux line is anisotropic depending on the field direction against the crystal axes[54]. Recently, for Bi2212, a new flux

line state so called a vortex chain was found for the field direction within 25° from the layers[55], however the mechanism has not been yet undestood. At the high temperature region, the flux line structure becomes uncertain due to thermal fluctuations[56].

In contrast to the above method, there are other techniques to examine the flux line state as follows; (1) Magneto-optical method, (2) Neutron diffraction method, (3) Shadow electron microscopy method, (4) Scanning tunneling microscopy (STM) method, (4) Electron holograpy method, and (5) DC transformer method. Further details of experimental techniques and other methods have been reviewed in Refs.[57,58].

1.4 Purpose of the present thesis

In the present thesis, transport critical currents and flux pinning properties in HTSC's are studied. The purpose of the present study is to understand the anisotropic nature in the mixed state related to their layered crystal structure and short coherence length. In order to investigate the intrinsic pinning properties and the two-dimensionality of the vortex motion due to the spatial variation of the order parameter along the c direction, systematic studies about the transport critical current density J_c are carried out using epitaxial thin films of YBCO and NCCO. In particular, J_c is measured as a function of the magnetic field B, their direction and temperature in a wide range. Since it is important for the study of the mixed state of HTSC's to consider the degree of the two-dimensionality of the materials, which depend on the temperature, obtained results are compared with other HTSC's with different degrees of the two-dimensionality such as Bi2212 etc.. Flux pinning mechanisms and the relation between the angular dependence of J_c and the two-dimensional vortex motion for each materials are discussed.

This thesis is composed of the following chapters except Introduction.

In chapter 2, some features of HTSC in the mixed state are summarized. Especially, this chapter focuses on the current matter in the mixed state, such as the transport critical current density, irreversibility line, intrinsic pinning effect and anisotropic vortex state.

In chapter 3, experimental procedures, such as preparation of YBCO and NCCO epitaxial thin films and transport critical current measurement in magnetic fields, are described.

In chapter 4, the temperature dependence of J_c on the magnetic field parallel to the ab plane is studied. Obtained J_c-T characteristics for YBCO and NCCO are analysed based on the intrinsic pinning model proposed by Tachiki and Takahashi. Using this model, the difference of the temperature dependence of J_c between YBCO and NCCO is discussed.

In chapter 5, the temperature dependence of the macroscopic Lorentz force effect and anisotropy of J_c are studied based on the concept for the 2D-3D dimensional crossover of superconducting properties. The angular dependence of J_c is also analysed using the critical state model. The relation between the anisotropy of J_c and dimensionality of each material is discussed assuming the stepwise vortex lines with strings and kinks. The temperature dependence of vortex dynamics and the dimensional crossover effect are also studied.

In chapter 6, the angular dependence of J_c and anisotropic pinning mechanisms are studied. J_c-B characteristics are analyzed by the flux pinning scaling law and pinning mechanisms are discussed. The anisotropy of J_c and the volume pinning force for YBCO and NCCO are examined. The obtained angular dependence of J_c is also analysed by using the Tachiki and Takahashi model, the 2D model and the scaling law of the flux pinning force considering the anisotropy of the irreversibility field.

Lastly, concluding remarks are described and the present thesis is summarized in chapter 7.

References

[1] J. G. Bednorz and Müller, *Z. Phys. B* **64** (1986) 189.

[2] R. J. Cava, R. B. van Dover, B. Batlogg and E. A. Rietman, *Phys. Rev. Lett.* **58** (1987) 408.

[3] H. Takagi, S. I. Uchida, K. Kitazawa and S. Tanaka, *Jpn. J. Appl. Phys.* **26** (1987) L1.

[4] J. M. Trascon, L. H. Greene, W. R. McKinnon, G. W. Hull and T. H. Geballe, *Science* **235** (1987) 1373.

[5] C. W. Chu, P. H. Hor, R. L. Meng, L. Gao and Z. J. Huang, *Science* **235** (1987) 567.

[6] C. N. Chu, P. H. Hor, R. L. Meng, L. Gao, Z. J. Huang and T. Q. Wang, *Phys. Rev. Lett.* **58** (1987) 405.

[7] M. K. Wu, J. R. Ashburn, C. J. Torng, P. H. Hor, R. L. Meng, L. Gao, Z. J. Huang, Y. Q. Wang and C. W. Chu, *Phys. Rev. Lett.* **58** (1987) 908.

[8] H. Maeda, Y. Tanaka, M. Fukutomi and T. Asano, *Jpn. J. Appl. Phys.* **27** (1988) L209.

[9] C. Michel, M. Hervieu, M. M. Borel, A. Grandin, F. Deslandes, J. Provost and B. Raveau, *Z. Phys. B* **68** (1987) 421.

[10] J. Akimitsu, A. Yamazaki, H. Sawa and H. Fujiki, *Jpn. J. Appl. Phys.* **26** (1987) L2080.

[11] Z. Z. Sheng and A. M. Hermann, *Nature* **332** (1988) 55.; *ibid.*, **332** (1988) 138.

[12] Z. Z. Sheng, A. M. Hermann, A. El Ali, C. Almasan, J. Estrada, T. Datta and R. J. Matson, *Phys. Rev. Lett.* **60** (1988) 937.

[13] R. M. Hazen, L. W. Finger, R. J. Angel, C. T. Prewitt, R. L. Ross, C. G. Hadidiacos, P. J. Heaney, D. R. Veblen, Z. Z. Sheng, A. El Ali and A. M. Hermann, *Phys. Rev. Lett.* **60** (1988) 1657.

[14] S. S. P. Parkin, V. Y. Lee, A. I. Nazal, R. Savoy, R. Beyers and J. La Placa, *Phys. Rev. Lett.* **61** (1988) 750.

[15] Y. Tokura, H. Takagi and S. Uchida, *Nature* **337** (1989) 345.

[16] H. Takagi, S. Uchida and Y. Tokura, *Phys. Rev. Lett.* **62** (1989) 1197.

[17] A. Schilling, M. Cantoni, J. D. Guo and H. R. Ott, *Nature* **363** (1993) 56.

[18] S. N. Putlin, E. V. Antipov, O. Chmaissem and M. Marezio, *Nature* **362** (1993) 226.

[19] J. R. Clem, *Phys. Rev. B* **43** (1991) 7837.

[20] M. Tachiki and S. Takahashi, *Solid State Commun.* **70** (1989) 291.

[21] D. Feinberg and C. Villard, *Phys. Rev. Lett.* **65** (1990) 919.

[22] B. I. Ivlev and N. B. Kopnin, *J. Low Temp. Phys.* **77** (1989) 419.

[23] A. Barone, A. I. Larkin and Yu. N. Ovchinnikov, *J. Supercond.* **3** (1990) 155.

[24] M. Tachiki and S. Takahashi, *Solid State Commun.* **72** (1989) 1083.

[25] F. Beech, S. Miraglia, A. Santro and R. S. Roth, *Phys. Rev. B* **35** (1987) 8778.

[26] F. Izumi, Y. Matsui, H. Takagi, S. Uchida, Y. Tokura and H. Asano, *Physica C* **158** (1989) 433.

[27] A. Yamamoto, M. Onoda, E. Takayama-Muromachi, F. Izumi, T. Ishigaki and H. Asano, *Phys. Rev. B* **42** (1990) 4228.

[28] A. A. Abrikosov, *Soviet Phys. JETP* **5** (1957) 20.

[29] V. L. Ginzburg and L. D. Landau, *Zh. Exper. Teor. Fiz.* **20** (1950) 1064.

[30] C. P. Bean, *Phys. Rev. Lett.* **8** (1962) 250.

[31] H. London, *Phys. Lett.* **6** (1963) 162.

[32] Y. B. Kim, C. F. Hempstead and A. R. Strnad, *Phys. Rev.* **129** (1963) 528.

[33] A. M. Campbell, J. E. Evett and D. Dew-Hughes, *Philos. Mag.* **10** (1964) 333.

[34] P. W. Anderson, *Phys. Rev. Lett.* **9** (1962) 309.

[35] J. Silcox and R. W. Rollins, *Appl. Phys. Lett.* **2** (1963) 231.; *Rev. Mod. Phys.* **36** (1964) 52.

[36] J. Friedel, P. G. de Gennes and J. Matricon, *Appl. Phys. Lett.* **2** (1963) 119.

[37] W. A. Fietz, M. R. Beasley, J. Silcox and W. W. Webb, *Phys. Rev.* **136 A** (1964) 335.

[38] K. Yasukouch, T. Ogasawara, N. Usui and S. Ushio, *J. Phys. Soc. Jpn.* **19** (1964) 1649.; *J. Phys. Soc. Jpn.* **21** (1966) 89.

[39] S. H. Goedemoed, P. H. Kes, F. Th. A. Jacobs and D. de Klerk, *Physica* **35** (1967) 273.

[40] T. H. Alden and J. D. Livingston, *J. Appl. Phys.* **37** (1966) 3551.

[41] A. M. Campbell, J. E. Evett and D. Dew-Hughes, *Philos. Mag.* **18** (1968) 313.

[42] H. T. Coffey, *Phys. Rev.* **166** (1968) 447.

[43] F. Irie and K. Yamafuji, *J. Phys. Soc. Jpn.* **23** (1967) 255.

[44] W. A. Fietz and W. W. Webb, *Phys. Rev.* **178** (1969) 657.

[45] R. G. Hampshire and M. T. Taylor, *J. Phys. F: Metal Phys.* **2** (1972) 89.

[46] C. P. Bean, *Rev. Mod. Phys.* **36** (1964) 36.

[47] A. M. Campbell, *J. Phys. C* **2** (1969) 1492.

[48] H. Küpfer, I. Apfelstedt, W. Schauer, R. Flükiger, R. Meier-Hirmer and H. Wühl, *Z. Phys. B* **69** (1987) 159.

[49] B. Ni, T. Munakata, T. Matsushita, M. Iwakuma, K. Funaki, M. Takeo and K. Yamafuji, *Jpn. J. Appl. Phys.* **27** (1988) 1658.

[50] Y. B. Kim, C. F. Hempstead and A. R. Strnad, *Phys. Rev. Lett.* **9** (1962) 306.

[51] H. Träuble and U. Essmann, *Phys. Status Solidi* **18** (1966) 813.

[52] G. J. Dolan, G. V. Chandrashekhar, T. R. Dinger, C. Feild and F. Holtzberg, *Phys. Rev. Lett.* **62** (1989) 827.

[53] L. Ya. Vinnikov, L. A. Gurevich, I. V. Grigoryeva, A. E. Koshele and Yu. A. Osipyan, *J. Less. Comm. Met.* **164 & 165** (1990) 1271.

[54] G. J. Dolan, F. Holtzberg, C. Feild and T. R. Dinger, *Phys. Rev. Lett.* **62** (1989) 2184.

[55] C. A. Bolle, P. L. Gammel, D. G. Grier, C. A. Murray, D. J. Bishop, D. B. Mitzi and A. Kapitulnik, *Phys. Rev. Lett.* **66** (1991) 7837.

[56] R. N. Kleiman, P. L. Gammel, L. F. Scheemeyer, J. V. Waszcza and D. J. Bishop, *Phys. Rev. Lett.* **62** (1989) 2331.

[57] A. M. Campbell and J. E. Evetts, *Adv. Phys.*, **21** (1972) 199.

[58] R. P. Huebener, *Magnetic Flux Structures in Superconductors*, (Springer-Verlag, Berlin, 1979).

Chapter 2

Some features of HTSC in the mixed state

2.1 Critical current density

At the beginning of the high T_c story, it was reported that the critical current density determined by magnetization measurement (J_c^M) was as high as $10^5 - 10^6$ A/cm^2[1,2]. This result was obtained by the indirect method of the magnetization measurement using the Bean model[3]. However, the transport critical current density J_c was found to be smaller than J_c^M[4]. This could be ascribed to the existence of weak links due to the granularity and weak intergrain contact in the polycrystalline sample[5]. In polycrystalline materials of HTSC, it has been found that there exist two sorts of critical current densities consisting of the intragrain critical current density and the intergrain one[6,7]. J_c^M is a mixture of two components of both inter- and intragrain critical current densities. On the contrary, the transport critical current density is limited by weak links at intra- or intergrain parts. Originally, the transport and magnetization critical current densities should be the same if the sample is of high quality. In fact, both critical current densities of YBCO epitaxial thin films were reported to be the same[8,9].

Fig.2.1 shows typical J_c's for various materials[10–15]. YBCO epitaxial thin films have the large J_c ($10^6 - 10^7$ A/cm^2) at both 77 K and 4.2 K[5,11,12]. J_c

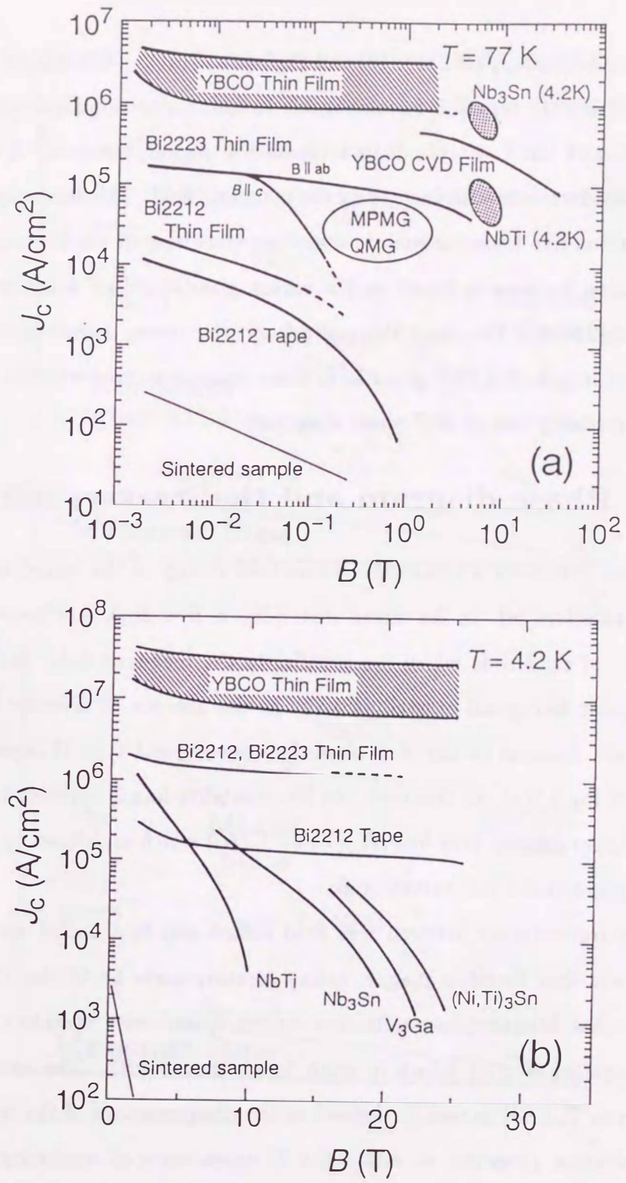

Fig. 2.1. Typical J_c as a function of the magnetic field for high T_c superconductors (a) at T = 77 K and (b) at T = 4.2 K. For comparison, data of conventional materials are shown.

for $Bi_2Sr_2CaCu_2O_{8+y}$ (Bi2212)[13] and $Bi_2Sr_2Ca_2Cu_3O_y$ (Bi2223)[14] epitaxial thin films, and Bi2212 tapes[15] is comparable to that for conventional superconductors at 4.2 K and 20 T. At the high temperature region, however, J_c for Bi-system drastically decreases with increasing the magnetic field. This fact may be connected with the flux line behavior such as a melting transition of the vortex lattice[16–18], a transition between a liquid and a vortex glass[19,20] or a thermally activated depinning[21–23]. The large thermal energy, the strong anisotropy and the short coherence length of HTSC give rise to these anomalous properties in the vicinity of an irreversibility line of B-T phase diagram.

2.2 Phase diagram and the irreversibility line

Abrikosov presented a remarkable mean field theory of the mixed state of type II superconductors[24]. In the mixed state ($B_{c1} < B < B_{c2}$), Abrikosov vortices have the form of rigid rods which are parallel to the magnetic field, and are arranged in a regular hexagonal crystalline array in the absence of disorder in the sample. The phase diagram in the B-T plane for conventional type II superconductors is shown in Fig.2.2(a). In this case, the irreversibility line is believed to be very close to the upper critical field line [$B_{c2}(T)$ or $T_c(B)$] which is defined by the mid point temperature of the ρ-T curves in B.

The irreversibility between zero field cooled and field cooled measurements on HTSC was first found in magnetization measurements by Müller *et al.*[25]. They showed that Meissner magnetization curves agreed with shielding ones down to a temperature $T_{irr}(B)$ which is much lower than $T_c(B)$. The irreversibility line [$B_{irr}(T)$ or $T_{irr}(B)$] is usually defined as the disappearance of the hysteresis in the magnetization property, at which the T dependence of resistivity drops to zero with decreasing T and the T dependence of critical current also drops zero with increasing T. Hence, the critical current density in the magnetic field becomes zero

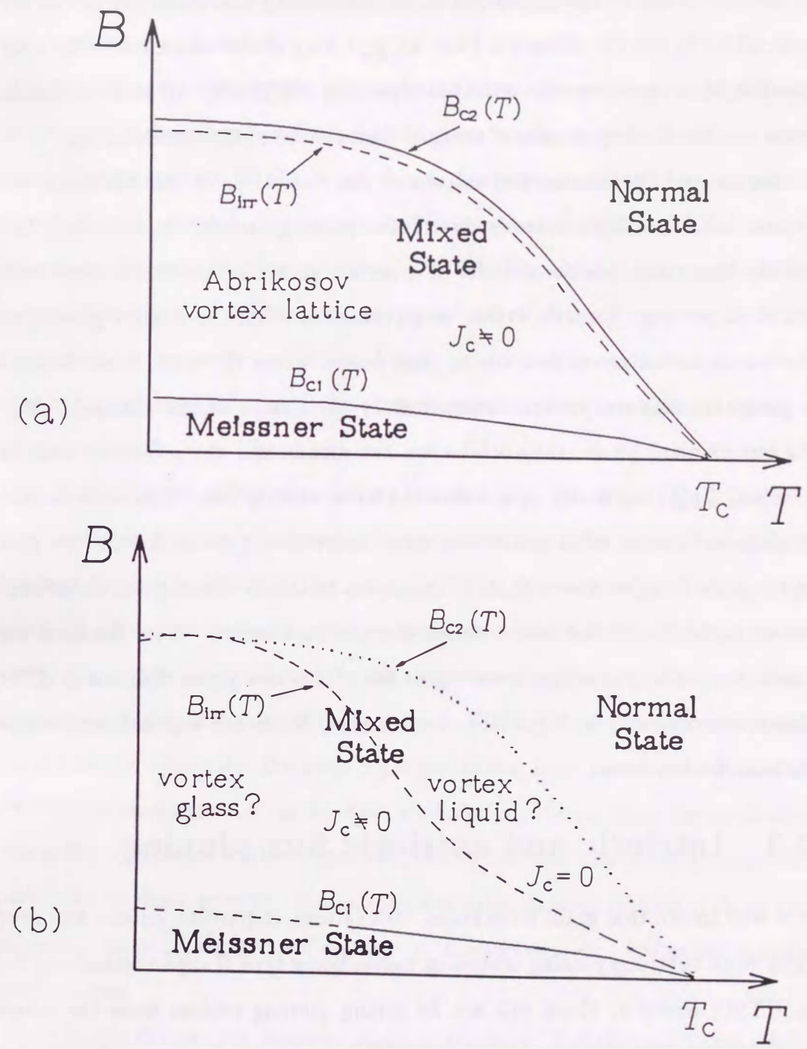

Fig. 2.2. Schematic illustration of the phase diagram in the B-T plane. (a) conventional type II superconductors and (b) high T_c superconductors.

not at $B_{c2}(T)$ line but at $B_{irr}(T)$ line in HTSC as shown in Fig.2.2(b). The origin of the irreversibility line is thought to be the melting transition line of the vortex lattice[16–18], the transition line from a liquid state of the vortex lattice to a vortex glass[19,20] or the thermally activated depinning line[21–23]. All these explanations point out the the importance of thermal fluctuations of the vortex lattice.

Larkin and Ovchinnikov[26] calculated the distortions of the Abrikosov vortex lattice due to weakly randomly distributed pinning centers. In this case, the infinitely long range positional order of a perfect vortex lattice is destroyed even by the weak pinning. Recently, it has been pointed out that the random pinning turns the vortex lattice phase to a vortex glass phase, where the vortices are frozen into a particular random pattern determined by the details of the pinning[19,20]. In the vortex glass phase, the vortices are not mobile and the resistivity defined by $\rho = \lim_{I\to 0}(\frac{dV}{dI})$ is strictly zero below the irreversibility line. This state is dissipationless and has an off-diagonal long range order analogous to that in spin glasses. In the high T region above $B_{irr}(T)$, the vortex lattice or vortex glass melts into the vortex liquid[16–20] due to the strong thermal fluctuations, where the local superconducting order parameter is driven to zero. This new phase diagram in HTSC is shown schematically in Fig.2.2(b). In this case, B_{c2} is not well defined because of thermal fluctuations.

2.3 Intrinsic and extrinsic flux pinning

It is well known that grain boundaries, dislocations, impurities, defects and precipitates work as strong pinning centers in conventional type II superconductors[27–29]. In HTSC, however, these will not be strong pinning centers from the following reasons.: (a) The coherence length of HTSC is very small compared with that of conventional materials. Since the vortex core size is small, the interaction between the vortex and pinning centers (so called core interaction) is thought to be small.

(b) The penetration depth of HTSC is large and internal magnetic field in the vortex lattice is almost uniform. Therefore, pinning force owing to the magnetic interaction is also considered to be small.

On the contrary, high quality epitaxial thin films have the large J_c of the order of 10^6 A/cm^2 as described in section 2.1 and these results indicate that some strong pinning centers exist in HTSC. It is a big problem what becomes strong pinning centers in high J_c samples. As the answer of the problem, Tachiki and Takahashi[30], Feinberg and Villard[31], Ivlev and Kopnin[32] and Barone *et al.*[33] suggested that the crystal structure of HTSC itself works as natural pinning centers. In HTSC, the superconducting order parameter $\Delta(r)$ is modulated along the c axis with the period of a_c, because CuO_2 layers are strongly superconductive and other layers are weakly superconductive. The values of a_c are 11.7 Å (= c), 6.0 Å (= $c/2$) and 15.3 Å (= $c/2$) for YBCO, NCCO and Bi2212, respectively. (See Fig.1.1 and Table 1.1) Figure 2.3 shows the spatial variation of superconducting order parameter along the c direction in the case of YBCO, for example. When two vortices exist at the points (a) and (b), the superconducting order parameter is modified from broken curve to the solid curve with a normal core. In the temperature region of $\xi_c(T) < a_c$, the loss of superconductive condensation energy due to the existence of vortex is the least when the vortex penetrates the weak superconducting layer at the point (b). Thus, the vortex becomes stable in the weak superconducting layers. Since the modulation of the order parameter works as natural pinning centers, this pinning mechanism is called the intrinsic pinning. In contrast, the other pinning centers such as grain boundaries, dislocations, impurities, defects, precipitates etc. are called extrinsic pinning centers.

In order to discuss the intrinsic pinning property, Tachiki and Takahashi[30] assumed the periodic spatial variation of the order parameter, $\Delta_0(z)$, as

$$\Delta_0(z) = \Delta_1 + \Delta_2 \cos\left(\frac{2\pi z}{a_c}\right) \quad , \tag{2.1}$$

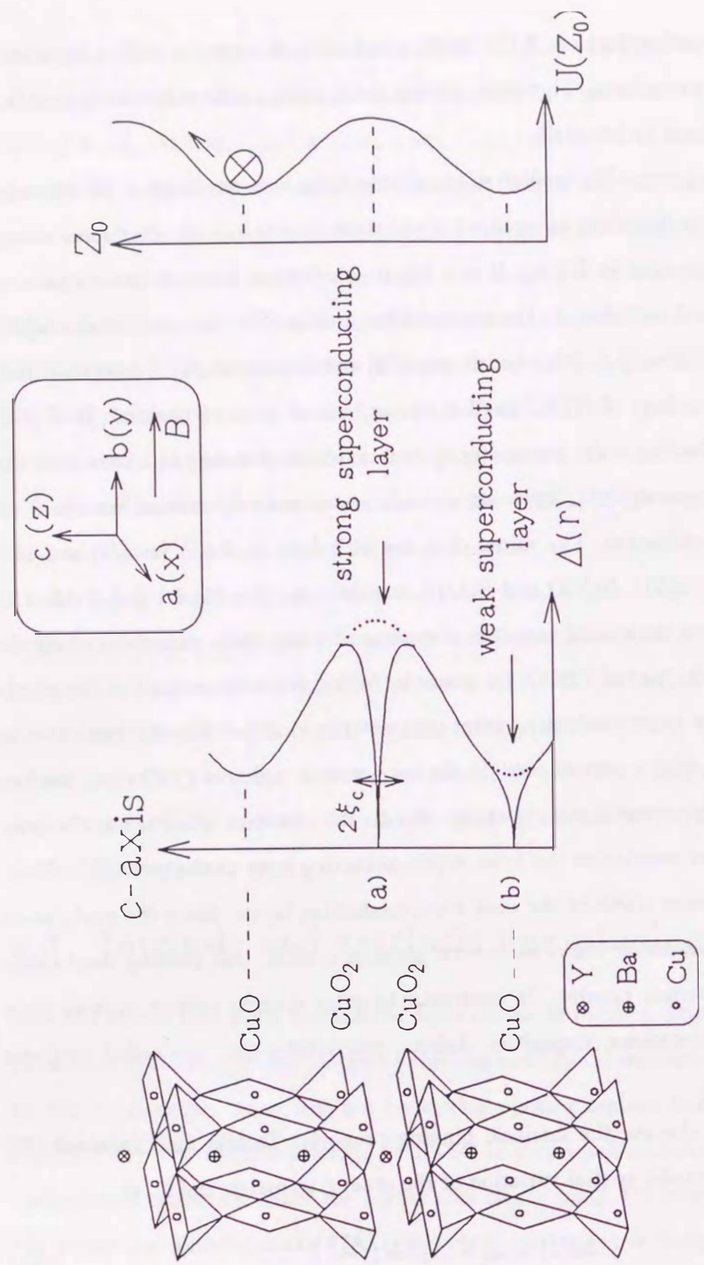

Fig. 2.3. Spatial variation of superconducting order parameter along the c-direction for YBCO.

where Δ_1 and Δ_2 are positive parameters with the relation of $\Delta_1 > \Delta_2$ and $z = 0$ is taken at an Y ion layer. As shown in Fig.2.3, the z axis is taken to be parallel to the c axis, and the x and y axes to be parallel to the a and b axes, respectively. Under the situation that one flux line is inserted along the y axis at the point (0, 0, z_0), the spatial variation of the order parameter is modified to the form[34],

$$\Delta(r) = \Delta_0(z) \tanh \left[\left(\frac{x}{\xi_{ab}} \right)^2 + \left(\frac{z - z_0}{\xi_c} \right)^2 \right]^{1/2}, \tag{2.2}$$

where $r = (x^2 + z^2)^{1/2}$. Using this relation, the difference of the condensation energy, $U(z_0)$, between state without and with one flux line is expressed as

$$U(z_0) = \frac{B_c^2}{\mu_0} \int dx dz \left[1 + \delta \cos \left(\frac{2\pi z}{a_c} \right) \right]^2 \mathrm{sech}^2 \left[\left(\frac{x}{\xi_{ab}} \right)^2 + \left(\frac{z - z_0}{\xi_c} \right)^2 \right]^{1/2}. \tag{2.3}$$

Here B_c is the thermodynamic critical field, μ_0 is the permeability of vacuum and δ is Δ_2/Δ_1. Equation (2.3) is a starting point to derive the elemental pinning force f_p, the volume pinning force F_p and the critical current density J_c[27]. For another application of the model, recently, Fukami *et al.*[35] calculate the temperature dependence of the activation energy, $\Delta U(T) = U(z_0 = 0) - U(z_0 = a_c/2)$, for YBCO, NCCO and Bi2212 using eq.(2.3) and obtained results are consistent with experimental ones.

In addition to the intrinsic pinning effect, recently, Tachiki *et al.*[36] proposed the following effect to enhance the pinning. When a transport current flows parallel to the layers, the current mainly flows in the strong superconducting layers. Then current density in the weak superconducting layers becomes much smaller than that in the strongly ones. They showed that each flux line is driven by the transport current density just at the flux line center, even when the flux line current spreads out over many layers. Therefore the driving force acting on the flux lines is much weaker than the force expected from the uniform current density, so this effect enhances the intrinsic pinning effect.

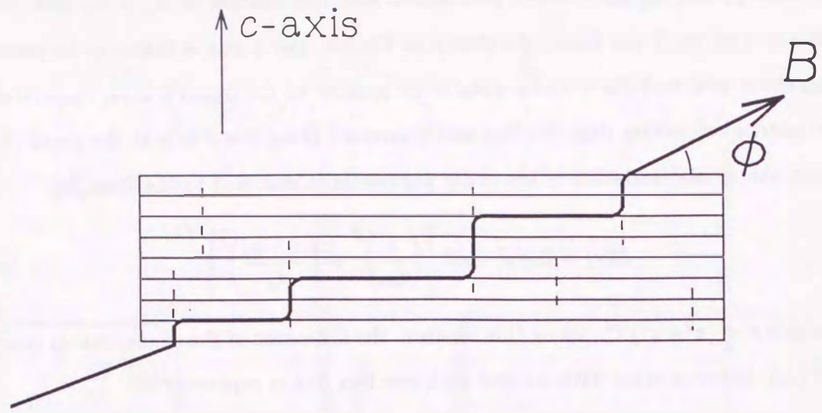

Fig. 2.4. Schematic drawing of a stepwise flux line in a sample. The bold solid line indicates a pass of the flux line core, and the horizontal lines and vertical dotted lines indicate the weak superconducting layers and extrinsic pinning centers, respectively.

The intrinsic pinning model described above is available only at the magnetic field direction parallel to the ab plane. However, when the magnetic field is applied at an angle ϕ, the extrinsic pinning centers must be considered. Here, ϕ is the angle between the magnetic field B and the ab plane under the condition of transport current $I \perp B$ (see Fig.2.4 and Fig.3.8). Since the intrinsic pinning is very strong, a stepwise flux line[30,31,37] would penetrate into the sample as shown in Fig.2.4. The bold solid line indicates a pass of the flux line core, and the horizontal lines and vertical dotted lines indicate the weak superconducting layers and extrinsic pinning centers, respectively. In this case, intrinsic pinning centers are effective for flux lines parallel to CuO_2 layers (namely strings) and extrinsic pinning centers are effective for those parallel to the c axis (namely kinks or pancakes). Assuming planer extrinsic pinning centers such as twin planes, Tachiki and Takahashi derived an angular dependence of J_c[38], which is given by

$$\frac{J_c(\phi)}{J_c(0^\circ)} = \frac{J_c(90^\circ)/J_c(0^\circ)}{|\sin\phi|^{1/2}} \quad , \tag{2.4}$$

under the condition of $D \gg a$. Here D is the average spacing between the twin planes and a is the lattice constant of triangular flux line lattice. Equation (2.4) has a sharp peak at $\phi = 0^\circ$ and the broad minimum at $\phi = 90^\circ$ and this tendency is similar to the experimental results for YBCO[39]. The similar feature of $J_c(\phi)$ would be obtained in other HTSC's such as NCCO and BSCCO.

2.4 Anisotropic properties of HTSC

Following the discovery of high-T_c oxide superconductors, it has been pointed out that they show a quasi-two-dimensional property due to their layered crystal structure and have much shorter anisotropic coherence lengths as compared with those of conventional superconductors. Until now, much effort has been made to investigate the anisotropic property of physical quantities such as the electrical resistivity ρ, the lower critical field B_{c1}, the upper critical field B_{c2}, the irreversibility field B_{irr}, the critical current density J_c and the volume pinning force F_p.

The determination of B_{c1} is difficult due to the surface pinning and the demagnetization effect, and also it is difficult to determine B_{c2} due to thermal fluctuations, nevertheless, the continuous study about these anisotropic nature has been performed. The anisotropic property of B_{c1} and B_{c2} is originated from the anisotropy of characteristic lengthes such as coherence lengths ξ and penetration depth λ. Within the framework of the anisotropic G-L theory, anisotropic B_{c1} and B_{c2} are expressed as[40],

$$B_{c1}^{(i)} = \frac{\phi_0}{4\pi\mu_0\lambda_j\lambda_k}\ln(\kappa_j\kappa_k)^{1/2} \quad , \tag{2.5}$$

$$B_{c2}^{(i)} = \frac{\phi_0}{2\pi\mu_0\xi_j\xi_k} \quad . \tag{2.6}$$

Here, i, j and k are coordinates used to express the direction of the crystal axes (a, b or c axes), and ϕ_0 is the flux quantum.

Table 2.1 summarizes the superconducting parameters for anisotropic HTSC

such as YBCO, NCCO and Bi2212 and conventional type II superconductors, Nb and Nb_3Sn. ρ_c/ρ_{ab} and $J_{c,ab}/J_{c,c}$ correspond to the transport current direction dependence of ρ and J_c , respectively at $B = 0$ T. The subscript denotes the direction of the transport current. The anisotropy of ρ[41,42] and J_c[43] for YBCO is smaller than those for Bi2212[44,45]. These parameters have not been obtained for NCCO.

Anisotropic values of B_{c2}, B_{c1}, ξ and λ at $T = 0$ K also have been obtained by a lot of experiments[46–62]. Here, ξ_{ab} and ξ_c are the Ginzburg-Landau coherence lengths for the directions parallel and perpendicular to the ab plane, respectively. λ_{ab} and λ_c are the penetration depths for the screening current directions parallel and perpendicular to the ab plane, respectively. The superscript denotes the direction of the applied magnetic field. The anisotropy of HTSC is expressed as the effective mass ratio,

$$\Gamma = \frac{m_c}{m_{ab}} = \frac{1}{\varepsilon^2} = \left(\frac{\xi_{ab}}{\xi_c}\right)^2 = \left(\frac{\lambda_c}{\lambda_{ab}}\right)^2 = \left[\frac{B_{c2}(\phi = 0°)}{B_{c2}(\phi = 90°)}\right]^2 . \tag{2.7}$$

Here, m_{ab} and m_c are the effective masses of the quasiparticles for the directions parallel and perpendicular to the ab plane, respectively. The anisotropy in the ab plane is ignored.

As first introduced by Lawrence and Doniach (LD)[63] and developed by Klemm, Luther and Beasley (KLB)[64], layered materials with $\xi_c \ll s$ are pictured as a stacked array of two dimensional superconducting layers which are weakly coupled by Josephson tunneling adjacent layers. Here, s is defined by the distance between the CuO_2 layers A crossover from three-dimensional (3D) properties to two-dimensional (2D) ones occurs when $\xi_c(T)$ becomes shorter than the critical layer spacing of $s/\sqrt{2}$ between the CuO_2 double layers. The dimensional crossover temperature T_{cross} is described by

$$T_{cross} = T_c \left[1 - \frac{2}{\Gamma}\left(\frac{\xi_{ab}(0)}{s}\right)^2\right] \tag{2.8}$$

$$= T_c \left[1 - 2\left(\frac{\xi_c(0)}{s}\right)^2\right] . \tag{2.9}$$

Table 2.1. Superconducting parameters of HTSC (YBCO, NCCO, Bi2212) and conventional type II superconductors (Nb, Nb_3Sn).

	YBCO	NCCO	Bi2212	Nb	Nb_3Sn
T_c (K)	90	24	85	9.25	18
ρ_c/ρ_{ab}	30 – 100	—	10^5	—	—
$J_{c,ab}/J_{c,c}$	10^2	—	10^3	—	—
$B_{c2}^{\perp c}(0)$ (T)	670 – 1200	137	530 – 2640	0.2	23
$B_{c2}^{\parallel c}(0)$ (T)	120 – 200	6.7	22 – 44		
$\xi_{ab}(0)$ (Å)	12 – 16	70 – 80	27 – 38	380	30
$\xi_c(0)$ (Å)	1.5 – 3	2 – 3	0.5 – 1.6		
$B_{c1}^{\perp c}(0)$ (Oe)	75	—	7	600	100
$B_{c1}^{\parallel c}(0)$ (Oe)	400	—	400		
$\lambda_{ab}(0)$ (Å)	1400	1000	2500 – 4500	390	650
$\lambda_c(0)$ (Å)	7000	—	—		

The anisotropy of ρ is given at the onset temperature of superconducting transition, and that of J_c is given at $T = 77$ K and $B = 0$. The lower and the upper critical field, the coherence length and the penetration depth are given at zero temperature.
Source: YBCO (ρ_c/ρ_{ab}[41,42], $J_{c,ab}/J_{c,c}$[43], B_{c2} and ξ[46–48], B_{c1} and λ[49–52]). NCCO (B_{c2} and ξ[53,54], B_{c1} and λ[55]). Bi2212 (ρ_c/ρ_{ab}[44], $J_{c,ab}/J_{c,c}$[45], B_{c2} and ξ[56,57], B_{c1} and λ[58–60]). Nb[61]. Nb_3Sn[62].

Table 2.2. The dimensional crossover temperature in HTSC.

	$\Gamma = \left[\frac{\xi_{ab}(0)}{\xi_c(0)}\right]^2$	$\xi_c(0)$ (Å)	s (Å)	$\frac{\xi_c(0)}{s}$	$T_{\rm cross}$
YBCO	30	1.5 – 3.0	8.3	0.18 – 0.36	(0.74 – 0.93) T_c
NCCO	900	2.0 – 3.0	6.1	0.33 – 0.49	(0.52 – 0.78) T_c
Bi2212	3000	0.5 – 1.6	12	0.04 – 0.13	(0.97 – 0.99) T_c

Since Bi2212 has very large Γ (=3000)[65], dimensional crossover occurs a few mK below T_c . In YBCO with $\Gamma = 30$[66], the 3D temperature region extends further to roughly $10 - 25$ K below T_c. Although NCCO has large Γ (=900)[54], the 3D region was calculated to be wide because of the large value of $\xi_c(0)/s$. The dimensional crossover temperatures for YBCO, NCCO and Bi2212 are summarized in Table 2.2.

One of the experimental evidences for the dimensionality was obtained from the angular dependence of $B_{c2}(\phi)$ for various anisotropic superconductors. For example, $B_{c2}(\phi)$ of Bi2212[67] and granular Aℓ thin films with a thickness $d < \xi$[68] conforms with the 2D-Tinkham model which is expressed as

$$\left|\frac{B_{c2}(\phi)\sin\phi}{B_{c2}(90°)}\right| + \left[\frac{B_{c2}(\phi)\cos\phi}{B_{c2}(0°)}\right]^2 = 1 \quad . \tag{2.10}$$

However, that of YBCO[69] and transition-metal dichalcogenide NbS_2[70] is described by the 3D-effective mass (anisotropic G-L) model which is expressed as

$$B_{c2}(\phi) = \frac{B_{c2}(90°)}{\sqrt{\sin^2\phi + \varepsilon^2\cos^2\phi}} \quad , \tag{2.11}$$

where ε is an effective mass ratio in eq.(2.7).

For a large value of Γ, the vortex state in HTSC has quite different properties as compared to that in conventional superconductors. For example, to study the vortex property in Bi2212 a quasi-2D approach is required. However, for YBCO it seems reasonable to treat it in the framework of an anisotropic G-L theory in the relatively wide temperature region. In the latter case, although the vortices are

considered as flux line, they have an anisotropic vortex lattice and elastic constants. When the magnetic field is parallel to the c axis a triangular Abrikosov lattice exists with a lattice parameter $a_0 = 1.075\,(\phi_0/B)^{1/2}$, the usual shear modulus c_{66} and the reduced tilt modulus c_{44} roughly by a factor Γ^{-1}[71]. The Abrikosov vortex becomes disordered due to the pinning by randomly distributed defects. The reduction of c_{44} causes a decrease of the longitudual correlation length L_c of the vortex[72]. When the magnetic field is parallel to the ab plane, very anisotropic c_{66} and c_{44}, and the vortex lattice with lattice parameters, $\sim a_0\Gamma^{\frac{1}{4}}$ and $a_0\Gamma^{-\frac{1}{4}}$, are expected[73–76], because the energy of deformations parallel to the ab plane is smaller than that of other directions. Schematic illustrations of the vortex states in the anisotropic 3D case ($\xi_c > s$) and 2D case ($\xi_c \ll s$) for $B \parallel c$ and $B \parallel ab$ are shown in Fig.2.5.

In the highly two dimensional case ($\xi_c \ll s$), Kes *et al.*[77] proposed that the concept of the Abrikosov vortex line would break down. Clem[78] also discussed the structure of vortex within a stack of superconducting layers, so called 2D pancake vortex. The screening currents are confined to the CuO_2 layers and lead to a segment of the 2D vortices as shown in Fig.2.5. The pancake vortex interacts with ones in adjacent superconducting layers by the electromagnetic dipole interaction, which tries to align the pancakes along the c axis, and by the interaction due to Josephson currents between the layers. At large angles between B and the ab plane ($\phi \sim 90°$, see Fig.2.5), a stack of pancake vortices is formed and only the field component parallel to the c axis is screened. In the angle smaller than $\phi = \tan^{-1}\Gamma^{1/2}$ the pancake vortices between two layers are linked by Josephson vortices (or Josephson strings)[79–81]. In this case the field parallel to the ab plane is partly screened, however, in a small angular regime ($\phi \sim 0°$) single Josephson vortices exist which are locked between the CuO_2 layers. When the vortex distance a_0 becomes smaller than the effective radius of the vortex (so called Josephson length $R_J = \Gamma^{1/2}s$), the parallel field component is not screened. When $a_0 = (\phi_0/B)^{1/2} < R_J$, *i.e.* $B > B_{2D} = \phi_0/\Gamma s^2$, the effectively decoupled pancake vortices show the two-dimensional

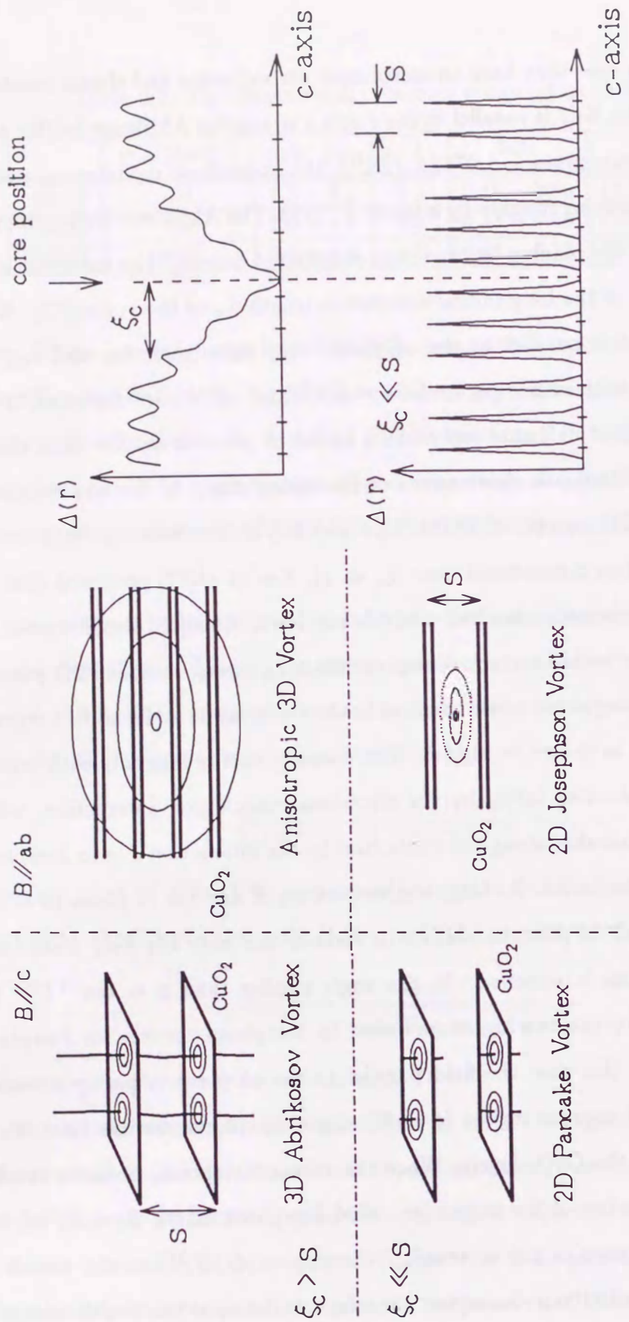

Fig. 2.5. Schematic illustration of the vortex state and the variation of the order parameter in the anisotropic 3D case ($\xi_c > s$) and 2D case ($\xi_c \ll s$) at $\phi = 0°$ and $\phi = 90°$.

behavior. The values of B_{2D} can be estimated as $B_{2D} \sim 0.3$ T for Bi2212 and 50 T for YBCO.

When the magnetic field is applied at the angle ϕ which is larger than the critical angle of the lock-in transition (that is kink creation angle ϕ_c), the relevant vortex properties are determined by the pancake vortices which can be treated as if a field $B \sin\phi$ is applied in the c direction. Since the angular dependence of the critical current is determined by the depinning of the pancakes, J_c is expressed by the scaling relation of the 2D model,

$$J_c(B, \phi) = J_{c\perp}(B \sin\phi) \quad , \tag{2.12}$$

where $J_{c\perp}(B)$ is $J_c(B)$ for $B \perp ab$. Using this relation $J_c(B, \phi)$ is calculated from the data of $J_c(B, 90°)$. In fact Schmitt *et al.*[82] showed that $J_c(B, \phi)$ for Bi2212 is well described by eq.(2.12) and the 2D pancake model seems to be valid in highly two-dimensional system.

References

[1] M. Oussena, S. Senoussi and G. Collin, *Europhys. Lett.* **4** (1987) 625.

[2] T. R. Dinger, T. K. Worthington, W. J. Gallagher and R. L. Sandstrom, *Phys. Rev. Lett.* **58** (1987) 2687.

[3] C. P. Bean, *Phys. Rev. Lett.* **8** (1962) 250.

[4] J. W. Ekin, A. I. Braginski, A. J. Panson, M. A. Janocko, D. W. Capone II, N. J. Zaluzec, B. Flandermeyer, O. F. de Lima, M. Hong, J. Kwo and S. H. Liou, *J. Appl. Phys.* **62** (1987) 4821.

[5] D. Dimons, P. Chaudhari, J. Mannhart and F. K. LeGoues, *Phys. Rev. Lett.* **61** (1988) 219.

[6] H. Küpfer, I. Apfelstedt, W. Schauer, R. Flükiger, R. Meier-Hirmer and H. Wühl, *Z. Phys. B* **69** (1987) 159.

[7] B. Ni, T. Munakata, T. Matsushita, M. Iwakuma, K. Funaki, M. Takeo and K. Yamafuji, *Jpn. J. Appl. Phys.* **27** (1988) 1658.

[8] P. Chaudhari, R. H. Koch, R. B. Raibowitz, T. R. McGuire and R. J. Gambino, *Phys. Rev. Lett.* **58** (1987) 2684.

[9] B. Oh, M. Naito, S. Arnason, P. Rosenthal, R. Barton, M. R. Beasley, T. H. Geballe, R. H. Hammond and A. Kapitulnik, *Phys. Rev. Lett.* **51** (1987) 852.

[10] *Nikkei Superconductors*, Japan, December 1989.; *ibid.*, February 1990.

[11] T. Nagaishi, H. Itozaki, T. Matsuura, N. Ota, N. Fujimori and S. Yazu, *Adv. Supercond. III, Proc. 3rd Int. Symp. Superconductivity, Sendai, 1990* (Springer-Verlag, Tokyo, 1991) p.921.

[12] G. Koren, A. Gupta, T. R. McGuire, *Appl. Phys. Lett.* **54** (1989) 1054.

[13] P. Schmitt, P. Kummeth, L. Schultz and G. Saemann-Ischenko, *Phys. Rev. Lett.* **67** (1991) 267.

[14] H. Yamasaki, K. Endo, S. Kosaka, M. Umeda, S. Yoshida and K. Kajimura, *Phys. Rev. Lett.* **70** (1993) 3331.

[15] K. Togano, H. Kumakura, D. R. Dietderich, H. Maeda, J. Kase and K. Nomura, *Adv. Supercond. III, Proc. 3rd Int. Symp. Superconductivity, Sendai, 1990* (Springer-Verlag, Tokyo, 1991) p.619.

[16] D. R. Nelson, *Phys. Rev. Lett.* **60** (1988) 1973.

[17] E. H. Brandt, *Phys. Rev. Lett.* **63** (1989) 1106.

[18] A. Houghton, R. A. Pelcovits and A. Sudbø, *Phys. Rev. B* **40** (1989) 6763.

[19] M. P. A. Fisher, *Phys. Rev. Lett.* **62** (1989) 1415.

[20] D. S. Fisher, M. P. A. Fisher and D. Huse, *Phys. Rev. B* **43** (1991) 130.

[21] Y. Yeshurun and A. P. Malozemoff, *Phys. Rev. Lett.* **60** (1988) 2202.

[22] A. P. Malozemoff, T. K. Worthington, Y. Yeshurun, F. Hortzberg and P. H. Kes, *Phys. Rev. B* **38** (1988) 7203.

[23] D. Dew-Hughes, *Cryogenics* **28** (1988) 637.

[24] A. A. Abrikosov, *Sov. Phys. JETP* **5** (1957) 1174.

[25] K. A. Müller, M. Takashige and J. G. Bednortz, *Phys. Rev. Lett.* **58** (1987) 1143.

[26] A. I. Larkin and Yu. N. Ovchinnikov, *J. Low Temp. Phys.* **34** (1979) 409.

[27] A. M. Campbell and J. E. Evetts, *Adv. Phys.* **21** (1972) 199.

[28] H. Ullmaier, *Irreversible Properties of Type II Superconductors*, (Springer-Verlag, Berlin, 1975).

[29] R. P. Huebener, *Magnetic Flux Structures in Superconductors*, (Springer-Verlag, Berlin, 1979).

[30] M. Tachiki and S. Takahashi, *Solid State Commun.* **70** (1989) 291.

[31] D. Feinberg and C. Villard, *Phys. Rev. Lett.* **65** (1990) 919.

[32] B. I. Ivlev and N. B. Kopnin, *J. Low Temp. Phys.* **77** (1989) 419.

[33] A. Barone, A. I. Larkin and Yu. N. Ovchinnikov, *J. Supercond.* **3** (1990) 155.

[34] M. Tinkham, *Introduction to Superconductivity*, (McGraw-Hill, New York, 1975) p.146.

[35] T. Fukami, K. Hayashi, T. Yamamoto, T. Nishizaki, Y. Horie, F. Ichikawa, T. Aomine, V. Soares and L. Rinderer, *Physica C* **184** (1991) 65.

[36] M. Tachiki, S. Takahashi and K. Sunaga, *Phys. Rev. B* **47** (1993) 6095.

[37] M. Tachiki, T. Koyama and S. Takahashi, *Physica C* **185-189** (1991) 303.

[38] M. Tachiki and S. Takahashi, *Solid State Commun.* **72** (1989) 1083.

[39] B. Roas, L. Schultz and G. Saemann-Ischenko, *Phys. Rev. Lett.* **64** (1990) 479.

[40] T. P. Orlando and K. A. Delin, *Foundations of Applied Superconductivity*, (Addison-Wesley, New York, 1991) p.303.

[41] Y. Iye, T. Tamegai, T. Sakakibara, T. Goto, N. Miura, H. Takeya and H. Takei, *Physica C* **155** (1988) 26.

[42] J. Z. Wu, P. Y. Hsieh, A. V. McGuire, D. L. Schmidt, L. T. Wood, Y. Shen and W. K. Chu, *Phys. Rev. B* **44** (1991) 12643.

[43] Y. Enomoto, T. Murakami, M. Suzuki and K. Moriwaki, *Jpn. J. Appl. Phys.* **26** (1987) L1248.

[44] S. Martin, A. T. Fiory, R. M. Fleming, L. F. Schneemeyer and J. V. Waszczak, *Phys. Rev. Lett.* **60** (1988) 2194.

[45] S. Martin, A. T. Fiory, P. M. Fleming, G. P. Espinosa and A. S. Cooper, *Appl. Phys. Lett.* **54** (1989) 72.

[46] U. Welp, W. K. Kwok, G. W. Crabtree, K. G. Vandervoot and J. Z. Liu, *Phys. Rev. Lett.* **62** (1989) 1908.

[47] M. Hikita and M. Suzuki, *Phys. Rev. B* **39** (1989) 4756.

[48] Y. Matsuda, T. Hirai, S. Komiyama, T. Terashima, Y. Bando, K. Iijima, K. Yamamoto and K. Hirata, *Phys. Rev. B* **40** (1989) 5176.

[49] L. Krusin-Elbaum, R. L. Greene, F. Holtzberg, A. P. Malozemoff and Y. Yeshurun, *Phys. Rev. Lett.* **62** (1989) 217.

[50] S. Sridhar, Dong-Ho Wu and W. Kenney, *Phys. Rev. Lett.* **63** (1989) 1873.

[51] D. H. Harshman, L. F. Schneemeyer, J. V. Waszczak, G. Aeppli, R. J. Cava, B. Batlogg and L. W. Rupp, *Phys. Rev. B* **39** (1989) 851.

[52] D. H. Harshman, A. T. Fiory and R. J. Cava, *Phys. Rev. Lett.* **66** (1991) 3313.

[53] Y. Hidaka and M. Suzuki, *Nature* **338** (1989) 635.

[54] M. Suzuki and M. Hikita, *Phys. Rev. B* **41** (1990) 9566.

[55] D. H. Wu, J. Mao, S. N. Mao, J. L. Peng, X. X. Xi, T. Venkatesan, R. L. Greene and S. M. Anlage, *Phys. Rev. Lett.* **70** (1993) 85.

[56] T. T. M. Palstra, B. Batlogg, L. F. Schneemeyer, R. B. van Dover and J. V. Waszczak, *Phys. Rev. B* **38** (1988) 5102.

[57] M. J. Naughton, R. C. Yu, P. K. Davies, J. E. Fischer, R. V. Chamberlin, Z. Z. Wang, T. W. Jing, N. P. Omg and P. M. Chaikin, *Phys. Rev. B* **38** (1988) 9280.

[58] S. Mitra, J. H. Cho, W. C. Lee, D. C. Johnston and V. G. Kogan, *Phys. Rev. B* **40** (1989) 2674.

[59] D. H. Harshman, R. N. Kleiman, M. Inui, G. P. Espinosa, D. B. Mitzi, A. Kapitulnik, T. Pfiz and Ll. Williams, *Phys. Rev. Lett.* **67** (1991) 3152.

[60] P. H. Kes, in *Phenomenology and Application of High-Temperature Superconductors, Proc. Los Alamos Symposium, 1991*, eds. K. S. Bedell, M. Inui, D. Meltzer, J. R. Schrieffer and S. Doniach (Addison-Wesley, New York, 1992) p.390.

[61] T. van Duzer and C. W. Turner, *Principles of Superconductive Devices and Circuits*, (Elsevier North Holland, New York, 1981).

[62] T. P. Orlando and K. A. Delin, *Foundations of Applied Superconductivity*, (Addison-Wesley, New York, 1991) p.576.

[63] W. E. Lawrence and S. Doniach, in *Proceedings of the Twelfth International Conference on Low Temperature Physics, Kyoto, 1970*, edited by E. Kanda (Academic Press of Japan, 1971), p.361.

[64] R. A. Klemm, A. Luther and M. R. Beasley, *Phys. Rev. B* **12** (1975) 877.

[65] D. E. Farrell, S. Bonham, J. Foster, Y. C. Chang, P. Z. Jiang, K. G. Vandervoot, D. L. Lam and V. G. Kogan, *Phys. Rev. Lett.* **63** (1989) 782.

[66] D. E. Farrell, C. M. Williams, S. A. Wolf, N. P. Bansal and V. G. Kogan, *Phys. Rev. Lett.* **61** (1988) 2805.

[67] M. J. Naughton, R. C. Yu, P. K. Davies, J. E. Fischer, R. V. Chamberlin, Z. Z. Wang, T. W. Jing, N. P. Ong and P. M. Chaikin, *Phys. Rev. B* **38** (1988) 9280.

[68] T. Aomine and L. Rinderer, *J. Low Temp. Phys.* **11** (1973) 173.

[69] Y. Iye, T. Tamegai, T. Sakakibara, T. Goto, N. Miura, H. Takeya and H. Takei, *Physica C* **153-155** (1988) 26.

[70] K. Onabe, M. Naito and S. Tanaka, *J. Phys. Soc. Jpn.* **45** (1978) 50.

[71] A. Houghton, R. A. Pelcovits and A. Sudbø, *Phys. Rev. B* **40** (1989) 6763.

[72] P. H. Kes, J. van den Berg, in *Studies of High Temperature superconductors*, Vol.5, ed. A. Narlikar, (NOVA Science Publishers, New York, 1990) p.83.

[73] A. Sudbø and E. H. Brandt, *Phys. Rev. B* **43** (1990) 10482.

[74] A. Sudbø and E. H. Brandt, *Phys. Rev. Lett.* **66** (1991) 1781.

[75] V. G. Kogan and L. J. Campbell, *Phys. Rev. Lett.* **62** (1989) 1552.

[76] L. J. Campbell, M. N. Doria and V. G. Kogan, *Phys. Rev. Lett.* **62** (1989) 1552.

[77] P. H. Kes, J. Aarts, V. M. Vinokur and C. J. van der Beek, *Phys. Rev. Lett.* **64** (1990) 1063.

[78] J. R. Clem, *Phys. Rev. B* **43** (1991) 7837.

[79] V. M. Vinokur, P. H. Kes and A. E. Koshelev, *Physica C* **168** (1990) 29.

[80] D. Feinberg, *Physica C* **194** (1992) 126.

[81] L. N. Bulaevskii, M. Ledvij and V. G. Kogan, *Phys. Rev. B* **46** (1992) 366.

[82] P. Schmitt, P. Kummeth, L. Schultz and G. Saemann-Ischenko, *Phys. Rev. Lett.* **67** (1991) 267.

Chapter 3

Experimental Procedures

3.1 Preparation of $YBa_2Cu_3O_{7-\delta}$ Thin Films

Epitaxial YBCO thin films were prepared by an activated reactive coevaporation technique at Institute for Chemical Research, Kyoto University[1–4]. Y and Ba were individually evaporated by electron-beam guns (JEOL JEBG-102UB) and copper was evaporated by an almina crucible heated by a tungsten wire. The film growth rate was in the range of $0.8 - 4$ Å/s. The local oxygen pressure near the substrate surface was kept at $10^{-2} - 10^{-1}$ Torr, while the background pressure was held 10^{-5} Torr during the deposition. In order to obtain the high quality thin film, oxygen plasma was generated by RF power supply (13.56 MHz, 100 W). The substrate temperature during the deposition was kept at $680 - 700$ °C. Films were cooled after deposition, keeping the oxygen flow onto the substrate, and oxidation treatment was performed in 200 Torr – 1 atm oxygen pressure at 500 °C for 1 hour. The prepared samples were characterized by X-ray diffraction (XRD). The epitaxial growth of YBCO thin film prepared by the above mentioned coevaporation technique was confirmed by *in situ* reflection high energy electron diffraction (RHEED)[2,4].

The c axis of the YBCO thin film was perpendicular to (100) surface of $SrTiO_3$ single-crystalline substrate. The typical thin film consists of a 1200 Å thick and 400 μm wide strip line, and potential electrodes were placed 1 mm apart. These films were patterned by a metal mask during deposition as shown in Fig.3.1 (a).

Thin films for transport critical current measurement at the temperature range of $T = 4.2 - 60$ K were patterned to 50 μm width by the photolithography and wet etching technique. The reason why the current path is made small as possible is that an effect of joule heating becomes large under the high transport current. The contact pads were made by evaporated silver and silver leads of diameter 50 μm were attached to them by indium solder. With this sort of contact, terminals could be proof against the high transport current up to 1 A.

3.2 Preparation of $Nd_{2-x}Ce_xCuO_{4-\delta}$ Thin Films

NCCO thin films were prepared by a reactive coevaporation method at NTT Interdisciplinary Laboratories, Nippon Telegraph and Telephone Corporation[5]. Nd and Ce were individually evaporated by electron-beam guns and Cu was evaporated by an effusion cell. The film growth rate was about 1 Å/s. The oxygen gas pressure in the deposition chamber was about 2×10^{-4} Torr. In order to assist oxygen activation, low power RF (13.56 MHz) plasma was generated. The substrate temperature was kept at 780 °C during the deposition. After deposition, the temperature was slowly cooled at a rate of 5 °C/min. The prepared samples were characterized by XRD, high-resolution scanning electron microscope (SEM) and atomic force microscope (AFM).

The c axis of the NCCO thin film was perpendicular to (100) surface of $SrTiO_3$ single-crystalline substrate. The prepared thin films were about 2000 Å thick. Film thickness for individual samples was measured by DEKTAK II profile meter with resolution, 5 Å. The measured samples were 50 μm wide and potential electrodes were placed 2 mm apart. These films were patterned by photolithographic technique and Ar ion beam etching as shown in Fig.3.1 (b). The contact pads were made by evaporated gold or silver and gold leads of diameter 50 μm were attached to them by indium solder and/or silver conductive paste (#4922 made in E. I. DU PONT

de Nemours & Co. Inc.).

3.3 Electrical measurements

3.3.1 Measurement systems

The electrical resistivity ρ and the transport critical current I_c were measured by using a standard DC-four-probe method. The thin films prepared with the above mentioned process were mounted on a copper block, the size being $10\times9\times5$ mm^3, using GE7031 varnish or Apiezon-N grease as shown in Fig.3.2. The block diagram of the measurement system of the temperature T dependence of ρ is shown in Fig.3.3. In the measurement, the transport current density, $10-100$ A/cm^2, was supplied by the Keithley 238 current source and the voltage was measured by the digital multimeter (Advantest R6561) with a resolution of 10 nV. The temperature was measured with a calibrated carbon-glass thermometer (CGR-1-500 of Lakeshore cryotronics Inc.) or a calibrated Au+0.07 at.% Fe vs. Chromel thermocouple and was controlled by a computer through GPIB and DIO interfaces. The data of $\rho(T)$ were collected by using the computer.

The transport critical current density J_c was determined from the current-voltage characteristics (I-V curves) plotted by an X-Y recorder. The block diagram of the measurement of J_c is shown in Fig.3.4. J_c was defined as the current density at which an electric field of 1 μV/cm or 5 μV/cm appeared for YBCO or NCCO thin films, respectively. During the measurement, temperature was stabilized within ±10 mK by using a Lakeshore DRC-91CA temperature controller.

Under high magnetic fields, measurements were made in a superconducting magnet system produced by Oxford Instrument Limited with a 52 mm diameter bore. The block diagram of the system is shown in Fig.3.5. The cryomagnetic system consists of a superconducting NbTi/Nb_3Sn hybrid solenoid which produces a vertical magnetic field at a sample position within a sample space where the temperature

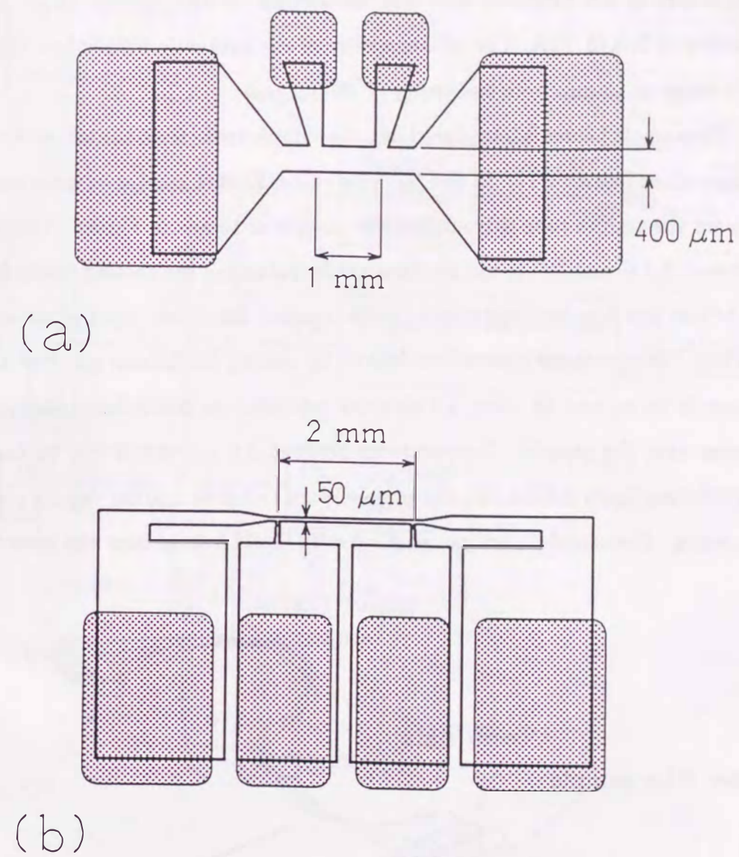

Fig. 3.1. Drawings of patterned thin films. (a)YBCO thin film and (b) NCCO thin film. The dotted regions represent silver electrodes.

is controlled. The magnitude of the magnetic field B was controlled by a sweep generator (SG-3). By increasing the current up to 101.9 A using a a current supply (PS120 : Max.120 A), it is possible to increase the magnetic field up to 12 T. The magnitude of the magnetic field was determined by the current value, using the relation of 0.1178 T/A. The inhomogenity of the magnetic field is less than 0.1 % in a range of 10 mm from the center of the magnet.

The sample holder is introduced into the sample space from the top of the variable temperature insert (VTI). In this holder a heater (100 Ω manganin wire) was wound around the copper tube surrounding the sample as shown in Fig.3.6. Temperatures between 4.2 K and 300 K can be obtained by balancing the cooling power by means of helium gas flow into the sample space, against the power input of the controller (ITC4). Temperature control is achieved by setting the helium gas flow rate with a needle valve, and by using a Lakeshore temperature controller connected to the heater near the sample. Temperatures between 2.0 and 4.2 K can be reached by introducing liquid helium into the sample space and reducing the vapour pressure by pumping. The sample space can be filled with liquid helium from the main reservoir

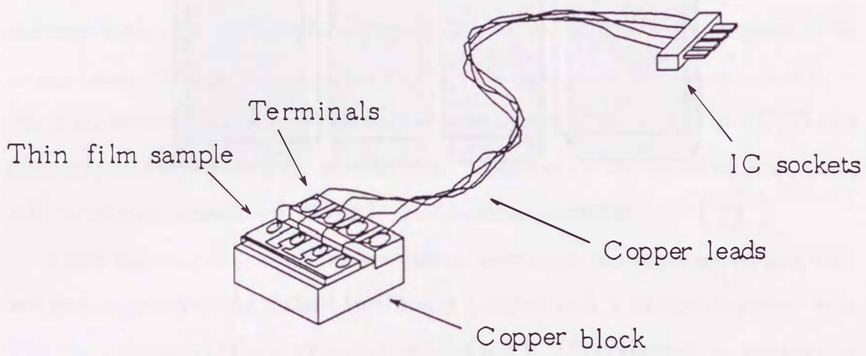

Fig. 3.2. Schematic drawing of a thin film sample mounted on a copper block.

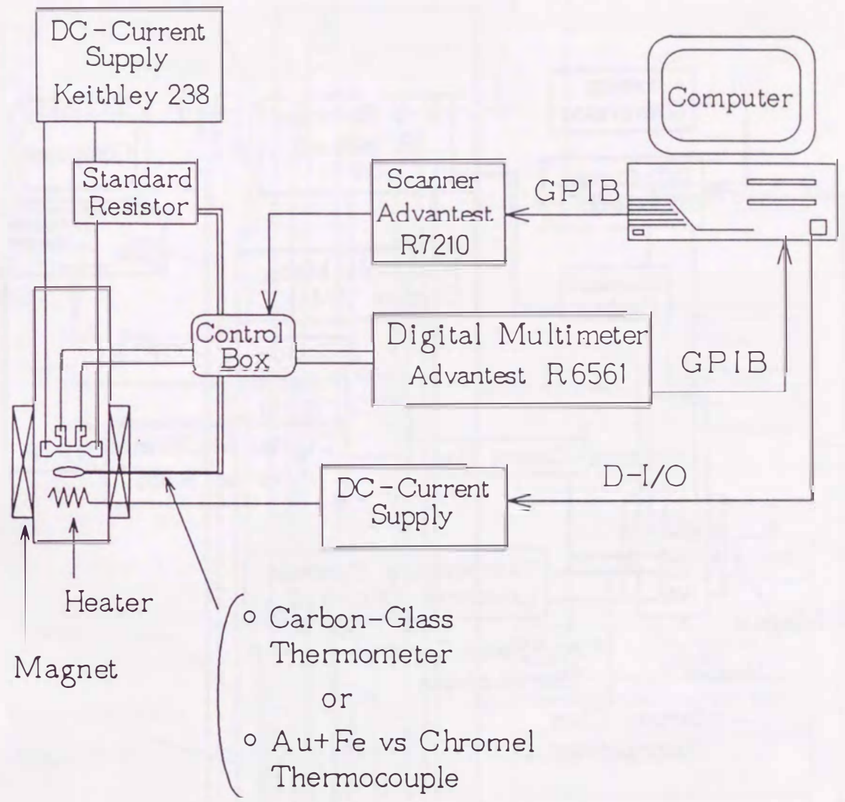

Fig. 3.3. Block diagram of the system for temperature dependence of electrical resistance measurements.

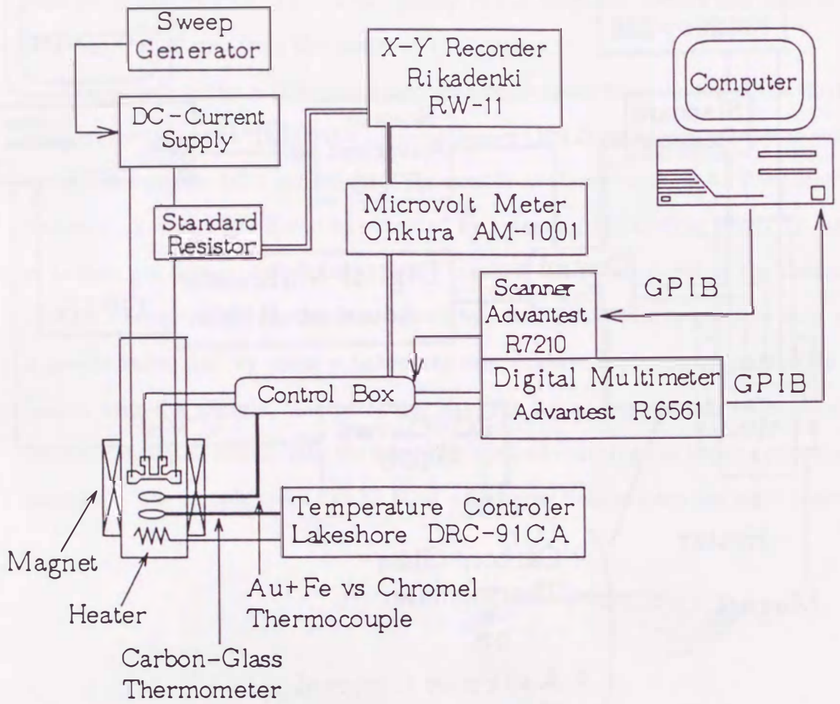

Fig. 3.4. Block diagram of the system for the transport critical current density measurement.

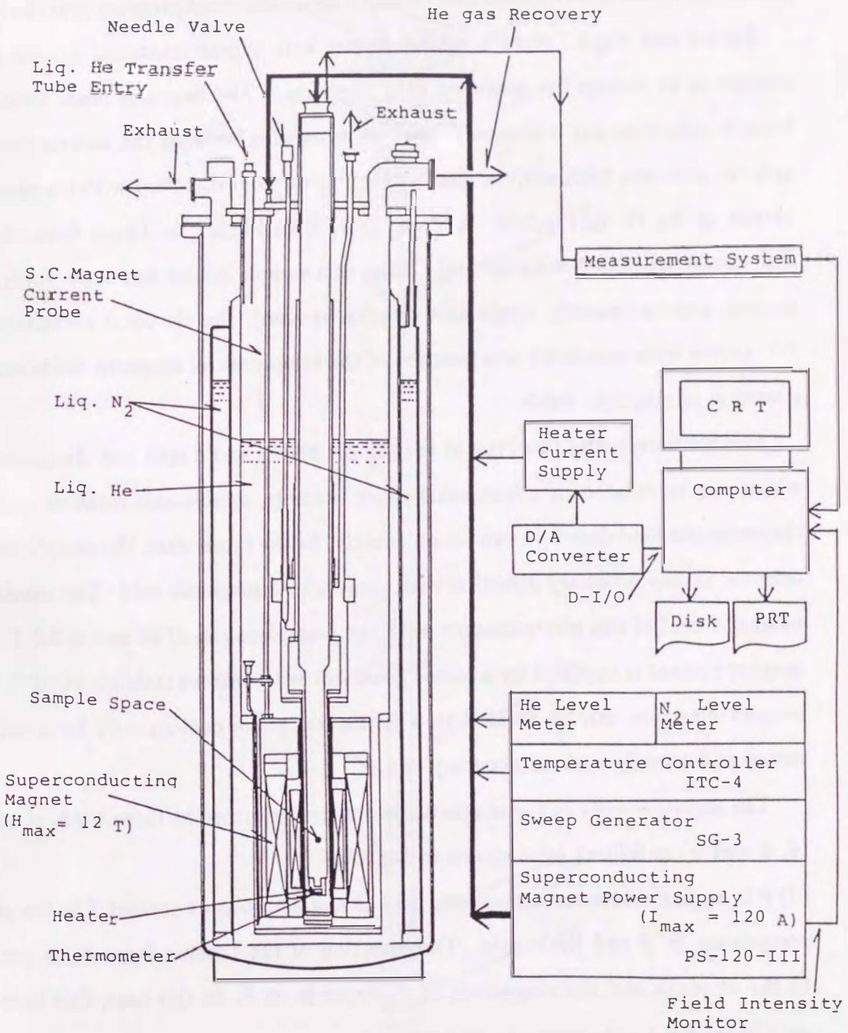

Fig. 3.5. Block diagram of the superconducting magnet system for the measurements under magnetic fields up to 12 T.

using the needle valve on the VTI top plate. In this case temperature control was performed by the use of a manostat to maintain a referenced pressure over the liquid.

Fig.3.6 and Fig.3.7 show a sample holder with a gear-rotational system which enables us to change the magnetic field direction. The device is made entirely of brass to minimize any difference of thermal expansion between the various parts. In order to minimize backlash, the gear is pulled toward one direction with the phosphor bronze spring (D in Fig.3.7). A worm gear, E in Fig.3.7, is driven from the top dial connected with a stainless rod. Using this sample holder and superconducting magnet system (namely, single-axis rotation system), the electrical resistivity and I-V curves were measured as a function of the temperature, magnetic fields and the direction of magnetic fields.

Furthermore, using this type of the sample holder and a split coil electromagnet which can be rotated in a horizontal plane (namely, double-axis rotation system), the magnetic field direction can be set exactly. In the latter case, the sample can be oriented in any arbitrary direction with respect to a magnetic field. The maximum magnetic field of this electromagnet with the pole-piece gap of 65 mm is 2.5 T. The magnet current is supplied by a motor generator with current stability of 10^{-4}. The magnet direction can be rotated in a horizontal plane continuously by a driving motor or manually with an accuracy of 0.1°.

The measurements in the magnetic field were performed at three kinds of angles (θ, ϕ and α) as follows (also shown in Fig.3.8):

(1) θ is an angle between a magnetic field B and a transport current I in the plane comprising B, I and the c axis. The direction of the Lorentz force F_L is parallel to the ab plane and the magnitude of F_L depends on θ. In this case, flux lines are mainly pinned by the extrinsic pinning centers.

(2) ϕ is an angle between B and the ab plane under the condition of $B \perp I$. The direction of F_L depends on ϕ, however the magnitude of F_L does not depend on ϕ. In this case, flux lines are pinned by both the extrinsic and the intrinsic pinning

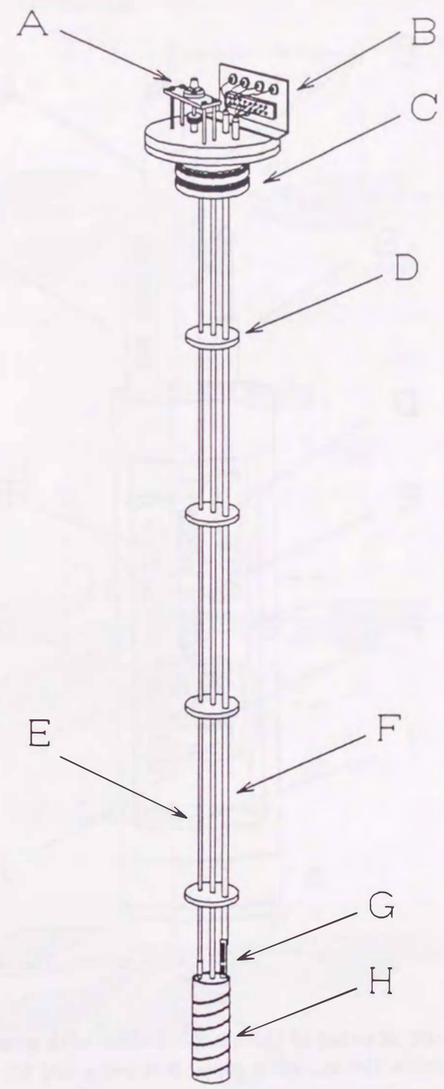

Fig. 3.6. Schematic drawing of the sample holder and attachments around them. A–dial for setting the sample direction; B–terminals; C–o-ring; D–radiation shield of stainless plate; E–driving rod for sample rotation; F–insulated leads inside the stainless pipe; G–IC sockets; H–heater.

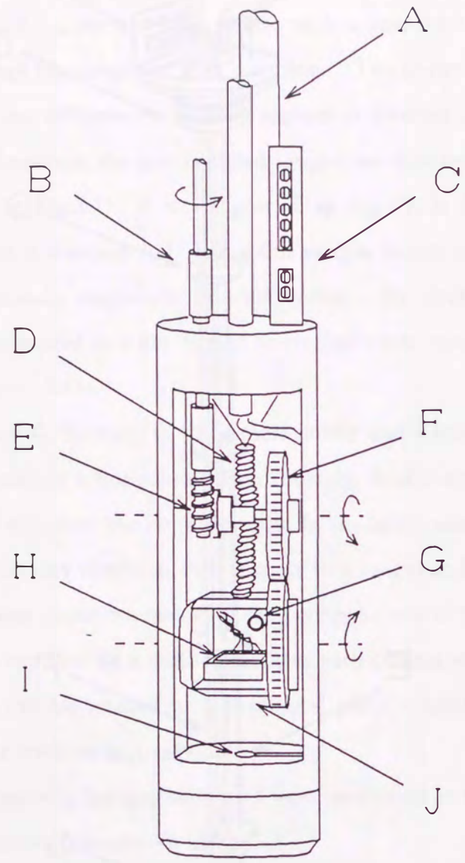

Fig. 3.7. Schematic drawing of the sample holder with gear-rotational system. A–insulated leads inside the stainless pipe; B–driving rod for sample rotation; C–IC sockets; D–phosphor bronze spring; E–worm gear; F–toothed gear; G–carbon-glass thermometer; H–sample; I–Au+0.07 at.% Fe vs. Chromel thermocouple; J–sample holder with toothed gear.

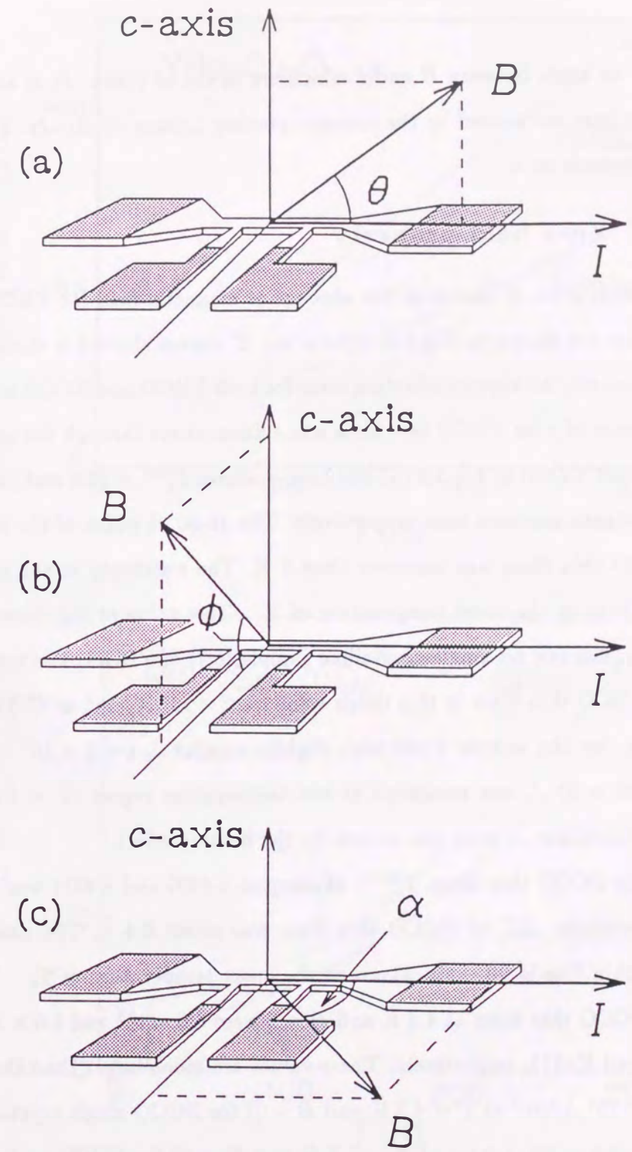

Fig. 3.8. Schematic drawing of the samples carrying transport current I under magnetic field B applied (a) at an angle θ, (b) at an angle ϕ and (c) at an angle α. The dotted regions represent silver electrodes.

centers.

(3) α is an angle between B and I which are in the ab plane. F_L is along the c axis and flux lines are pinned by the intrinsic pinning centers effectively. The magnitude of F_L depends on α.

3.3.2 Zero field property

The typical ρ vs. T curves in the absence of magnetic field for YBCO and NCCO thin films are shown in Fig.3.9. The ρ vs. T curves showed a sharp and smooth transition into the superconducting state for both YBCO and NCCO samples. The T dependence of ρ for YBCO thin films was a linear curve through the origin. Samples Y279B and Y325B in Fig.3.9 (a) had temperatures T_c^{zero} = 87.6 and 86.0 K at which the resistance becomes zero, respectively. The 10-90 % width of the transition ΔT_c of YBCO thin films was narrower than 1 K. The resistivity of the sample Y325B is 65 $\mu\Omega$·cm at the onset temperature of T_c . This value at the onset temperature shows typical one for single-crystalline samples[6,7] of YBCO. The typical values of J_c for YBCO thin films in this thesis were $1-2\times10^6$ A/cm^2 at 77.3 K and $B=0$. However, for the sample Y280 with slightly smaller J_c ($\sim 5\times10^5$ A/cm^2 at 77.3 K and $B=0$) J_c was measured at low temperature region ($T<60$ K), because samples with low J_c were not broken by the heating effect.

As for NCCO thin films, T_c^{zero}'s of samples K4305 and K4311 was 18.5 and 19.0 K, respectively. ΔT_c of NCCO thin films was about 0.4 K. The resistivity of the NCCO thin film is $30-50$ $\mu\Omega$·cm at the onset temperature of T_c . The values of J_c for NCCO thin films at 4.2 K and $B=0$ were 6.0×10^5 and 1.6×10^6 A/cm^2 for K4305 and K4311, respectively. These values are much larger than the value of J_c^M ($=1.5\times10^4$ A/cm^2 at $T=4.2$ K and $B=0$) for NCCO single crystals[8] and that of J_c ($=2.0\times10^5$ A/cm^2 at $T=5.5$ K and $B=0$) for NCCO epitaxial thin film prepared by the laser ablation technique[9].

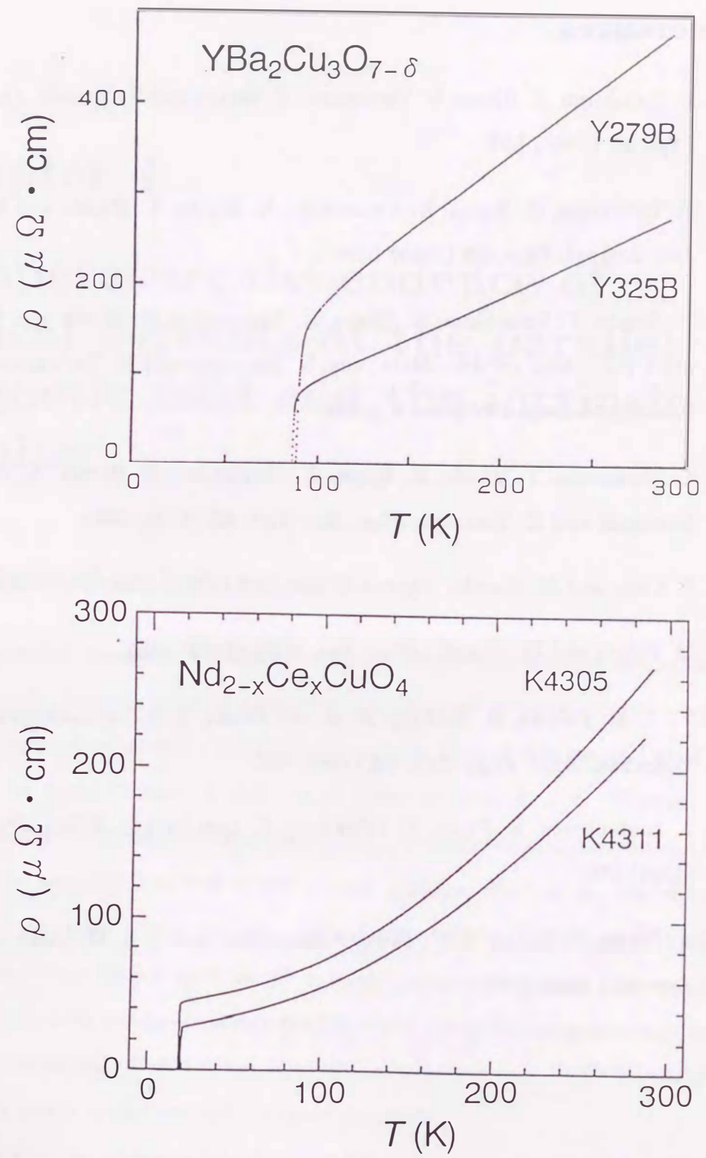

Fig. 3.9. T dependence of ρ for (a) YBCO and (b) NCCO thin films in the absence of a magnetic field.

References

[1] T. Terashima, K. Iijima, K. Yamamoto, Y. Bando and H. Mazaki, *Jpn. J. Appl. Phys.* **27** (1988) L91.

[2] T. Terashima, K. Iijima, K. Yamamoto, K. Hirata, Y. Bando and H. Mazaki, *Jpn. J. Appl. Phys.* **28** (1989) L987.

[3] Y. Bando, T. Terashima, K. Iijima, K. Yamamoto, K. Hirata and H. Mazaki, *MRS Int'l. Mtg. on Adv. Mats.*, eds. K. Kitazawa and K. Tachikawa (Material Research Society, 1989) Vol.6, p.731.

[4] T. Terashima, Y. Bando, K. Iijima, K. Yamamoto, K. Hirata, K. Hayashi, K. Kamigaki and H. Terauchi, *Phys. Rev. Lett.* **65** (1990) 2684.

[5] S. Kubo and M. Suzuki, *Physica C* **185-189** (1991) 1251.

[6] M. Hikita and M. Suzuki, *Phys. Rev. B* **39** (1989) 4756.

[7] T. T. M. Palstra, B. Batlogg, R. B. van Dover, L. F. Schneemeyer and J. V. Waszczak, *Appl. Phys. Lett.* **54** (1989) 763.

[8] J. Fontcuberta, S. Piñol, X. Obradors, F. Lera and C. Rillo, *Cryogenics* **30** (1990) 656.

[9] A. Gupta, G. Koren, C. C. Tsuei, A. Segmüller and T. R. McGuire, *Appl. Phys. Lett.* **55** (1989) 1795.

Chapter 4

Temperature dependence of critical currents at the parallel magnetic field and the intrinsic pinning

4.1 Introduction

Intrinsic pinning mechanism is one of the most important pinning mechanism in HTSC. Usually, intrinsic pinning properties are discussed in connection with a sharp peak of angular dependence of $J_c(\phi)$[1] or a sudden drop of resistance[2] at $B \parallel ab$. Here ϕ is an angle between B and the ab plane keeping $B \perp I$. However, it is difficult to analyze the angular dependence of J_c , because the extrinsic pinning effect also must be considered as well as the intrinsic pinning effect at the field direction of $\phi \neq 0°$. In order to describe the angular dependence, Tachiki and Takahashi assumed that twin planes work as the extrinsic pinning centers in the case of the YBCO and derived a theoretical equation[3]. Since the twin planes generally do not exist in the materials with tetragonal crystal structures, *e.g.*, NCCO, Bi2212 and LSCO, this model would not hold in these materials.

Considering the magnetic field direction fixed at $\phi = 0°$, the situation is thought to be simple. In this case, only the intrinsic pinning due to the layered structure would works as the strong pinning centers, because other extrinsic pinning centers

are not effective in this field direction. Therefore, the dependence of J_c on T at $\phi = 0°$ is closely related to the flux pinning dynamics due to the intrinsic pinning. Since the magnitude of the intrinsic pinning force depends on the coherence length in the c- direction $\xi_c(T)$ and the distance between the CuO_2 layers, the value and T dependence of J_c on B would vary with the variety of the materials. In spite of the essential configuration, the systematic study of the $J_c(B)$ - T property at $\phi = 0°$ has not been studied fully up to the present, because a preparation of high quality samples is difficult.

In this chapter, the behavior of $J_c(T, B)$ for high quality YBCO and NCCO thin films in $B \parallel ab$ is examined over a wide temperature range from 4.2 K to T_c. The obtained results are discussed based on the intrinsic pinning model proposed by Tachiki and Takahashi. If the intrinsic pinning mechanism holds, systematical difference of $J_c(T)$ between YBCO and NCCO would be observed.

4.2 Measurements

Measurements under the magnetic fields up to 12 T were performed at the configuration of $\phi = 0°$. The measured temperature was in the range of $10 - 80$ K ($4.2 - 19$ K) for YBCO (NCCO) thin films. A one cycle of the measurement was done at the constant magnetic field as a function of the temperature. In all measurements, temperature was stabilized within ± 10 mK. The direction of the field parallel to the ab plane was determined by the angular dependence of the critical current and was checked in the every cycle of the measurements. The deviation of the magnetic field direction from the ab plane was smaller than 0.1°.

In this chapter, the sample Y280 (K4311) was used as YBCO (NCCO) sample. T_c^{zero}'s of Y280 and K4311 was 87.0 and 19.0 K, respectively. J_c of K4311 shows 1.6×10^6 A/cm^2 at 4.2 K and 0 T, which is larger than other NCCO samples. The sample Y280 had slightly smaller J_c ($\sim 5 \times 10^5$ A/cm^2 at 77.3 K and $B = 0$) than

other YBCO thin films in this thesis. The other samples of YBCO were broken by the heating effect when J_c exceeded 10^7 A/cm^2 range at $T = 50 - 60$ K. Therefore these samples could not be measured at the low temperature region.

4.3 Results and discussion

4.3.1 Characteristics of $J_c(B)$ - T curves at $\phi = 0°$

Figure 4.1 shows temperature dependence of J_c for sample Y280A (YBCO thin film) under various magnetic fields B at $\phi = 0°$. At the temperature region below 30 K, J_c's are almost independent of the magnitude of B up to 12 T and change gradually with T. J_c at $T = 10$ K shows 6×10^6 A/cm^2. At the temperature region above 40 K, on the contrary, J_c's largely decrease with increasing B and T. At $T = 80$ K, especially, J_c at 12 T becomes three orders of magnitude smaller than J_c at 1T. These results indicate that the intrinsic pinning force becomes small with increasing the temperature.

A similar result was observed for sample K4311 (NCCO thin film) as shown in Fig.4.2. The temperature and magnetic field dependences of J_c for NCCO is large as compared with those for YBCO. The difference would result from the intrinsic pinning property for each material.

Awaji *et al.*[4] reported that the YBCO thin film prepared by the CVD method showed J_c - T curves with dip structures in the vicinity of the dimensional crossover temperature. However, such structures have not been observed in our both samples of YBCO and NCCO thin films.

4.3.2 Estimation of J_c based on the intrinsic pinning model

In order to estimate the value of J_c due to the intrinsic pinning and to describe the T dependence of J_c , let us apply the intrinsic pinning model by Tachiki and Takahashi[5] described in section 2.3. Again, assuming the same configurations as

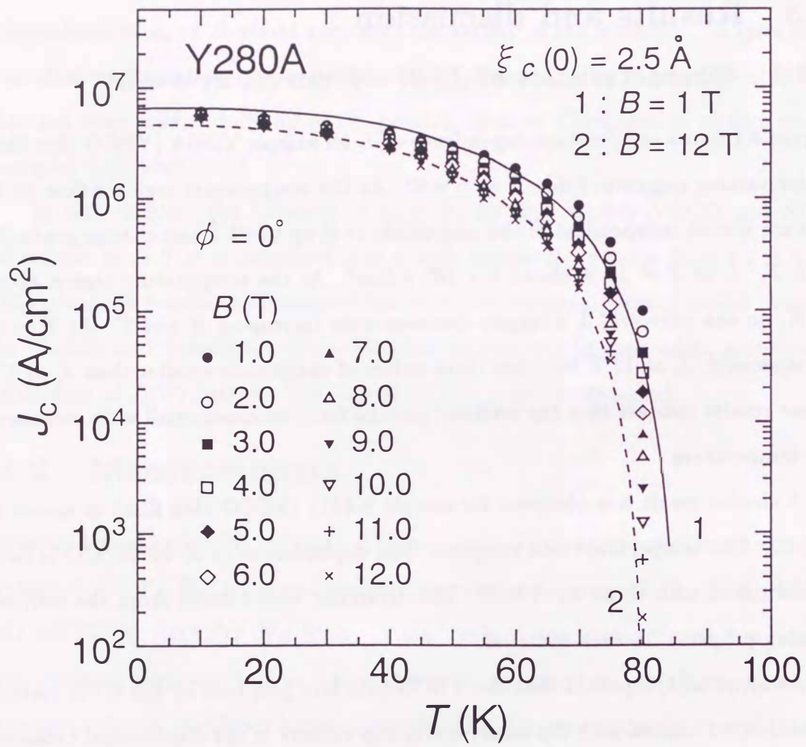

Fig. 4.1. Temperature dependence of J_c for sample Y280A (YBCO) under various magnetic fields at $\phi = 0°$. The solid and the broken curves were calculated for $B = 1.0$ T and 12.0 T in case of $\xi_c(0) = 2.5$ Å ($\xi_c(0)/a_c = 0.21$) using eq.(4.7).

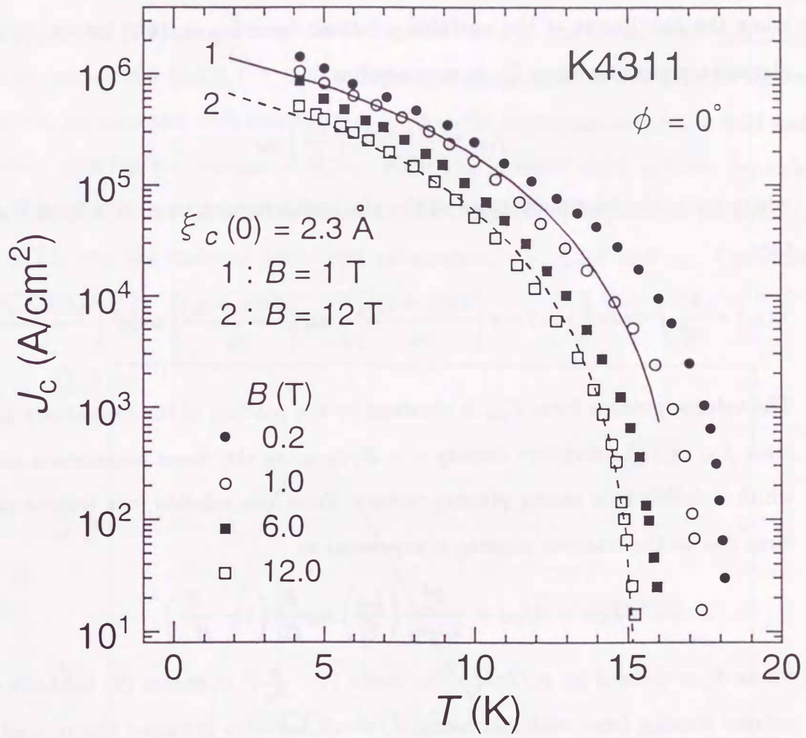

Fig. 4.2. Temperature dependence of J_c for sample K4311 (NCCO) under various magnetic fields at $\phi = 0°$. The solid and the broken curves were calculated for $B = 1.0$ T and 12.0 T in case of $\xi_c(0) = 2.3$ Å ($\xi_c(0)/a_c = 0.38$) using eq.(4.7).

that described in section 2.3, the force in the z direction is calculated by

$$f_p(z_0) = -\frac{d}{dz_0}U(z_0) \quad , \tag{4.1}$$

from the eq.(2.3). This force directs from an unstable position to a stable one when the flux line is at the unstable position. Inserting eq.(4.1) into eq.(2.3), the elementary pinning force $f_{\rm pM}$ is expressed as

$$f_{\rm pM} = \frac{B_c^2}{2\mu_0}2\pi a_c\left(\frac{\xi_{ab}}{\xi_c}\right)\eta_{\rm M} \quad , \tag{4.2}$$

where η_M is the maximum value of the $\eta(z_0)$ with respect to z_0 at a fixed temperature,

$$\eta(z_0) = \frac{4\delta}{a_c^2}\int dxdz\left(1+\delta\cos\left[\frac{2\pi(z+z_0)}{a_c}\right]\right)\sin\left[\frac{2\pi(z+z_0)}{a_c}\right]\mathrm{sech}^2\left(\frac{\sqrt{x^2+z^2}}{\xi_c}\right) \quad . \tag{4.3}$$

The volume pinning force $F_{\rm pM}$ is obtained by the product of the elementary pinning force $f_{\rm pM}$ and the flux line density $n = B/\phi_0$ using the direct summation method, which is fulfilled for strong pinning centers. From this relation, the volume pinning force due to the intrinsic pinning is expressed as

$$F_{\rm pM} = nf_{\rm pM} = \frac{B_c^2}{2\mu_0 a_c}\left(\frac{\xi_{ab}}{\xi_c}\right)\eta_{\rm M}\frac{B}{B_0}\left(1-\frac{B}{B_{c2}}\right)^2 \quad , \tag{4.4}$$

where B_0 is defined by $\phi_0/2\pi a_c^2$. The factor $(1-\frac{B}{B_{c2}})^2$ indicates the decrease of the volume pinning force with increasing B, which has been obtained theoretically[6–8] and experimentally[9,10]. For high T_c superconductors, B_{c2} must be substituted for the irreversibility field $B_{\rm irr}$ at which $F_{\rm pM}$ becomes zero. Finally, the critical current density at $\phi = 0°$ is obtained as

$$J_c(T,B) = \frac{F_{\rm pM}(T)}{B} = \frac{[B_c(T)]^2}{2\mu_0 a_c}\frac{1}{B_0}\left[\frac{\xi_{ab}(T)}{\xi_c(T)}\right]\eta_{\rm M}(T)\left[1-\frac{B}{B_{\rm irr}(T)}\right]^2 \tag{4.5}$$

$$= \frac{\pi a_c[B_c(0)]^2}{\mu_0\phi_0}\left[\frac{\xi_{ab}(0)}{\xi_c(0)}\right]\eta_M(T)\,(1-t^2)^2\left[1-\frac{B}{B_{\rm irr}(0)}\frac{1}{1-t^2}\right]^2 \tag{4.6}$$

$$\equiv J_{c0}\,\eta_M(T)\,(1-t^2)^2\left[1-b(0)\frac{1}{1-t^2}\right]^2 \quad . \tag{4.7}$$

Here, $B_c(T)$ is the temperature dependence of the thermodynamic critical field $B_c(T) = B_c(0)\,(1-t^2)$, t is defined by T/T_c, b is defined by $B/B_{\rm irr}$ and temperature dependence of the irreversibility field is assumed as $B_{\rm irr} = B_{\rm irr}(0)\,(1-t^2)$.

Figure 4.3 shows ξ_c/a_c dependence of $\eta_{\rm M}$ for $\delta = 0.6$. The value of $\eta_{\rm M}$ was obtained by the numerical integration of eq.(4.3) and it was found that $\eta_{\rm M}(\xi_c/a_c)$ for other values of δ (=0.2, 0.4, 0.8) is in proportion to that for $\delta = 0.6$. As shown in Fig.4.3, $\eta_{\rm M}$ increases with increasing ξ_c/a_c, has the maximum at $\xi_c/a_c \simeq 0.28$ and decreases with further increase of ξ_c/a_c. Since the intrinsic pinning force depends on $\xi_c(T)/a_c$, $J_c(T)$ would be determined by the temperature dependent parameter, *e.g.*, $\xi_c(T)$, and the material dependent parameters, *e.g.*, $\xi_c(0)$ and a_c. Therefore

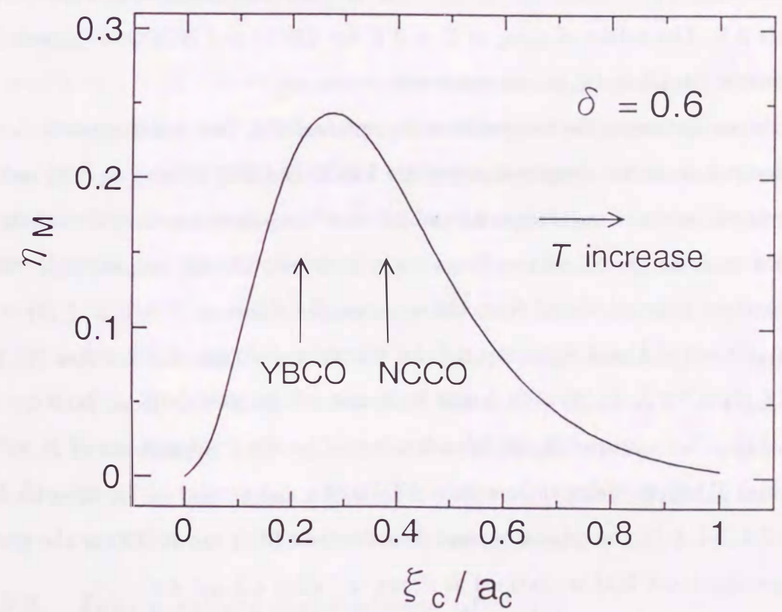

Fig. 4.3. $\xi_c(T)/a_c$ dependence of $\eta_{\rm M}$ for $\delta = 0.6$. The value of ξ_c/a_c at $T = 0$ K for YBCO and NCCO is expressed by arrows. ξ_c/a_c increases with increasing T.

Table 4.1. Parameters for estimating the value of J_c for YBCO.

T (K)	ξ_{ab} (Å)	ξ_c (Å)	B_c (T)	B_{irr} (T)	ξ_c/a_c	$\eta_M(\delta = 0.2, 0.4, 0.6)$
4.2	7.7	2.6	1.0	150	0.21	0.073, 0.15, 0.22
77.3	36.5	7.3	0.22	20	0.62	0.023, 0.047, 0.07

Table 4.2. Parameters for estimating the value of J_c for NCCO.

T (K)	ξ_{ab} (Å)	ξ_c (Å)	B_c (T)	B_{irr} (T)	ξ_c/a_c	$\eta_M(\delta = 0.2, 0.4, 0.6)$
4.2	78	2.6	0.19	38	0.43	0.057, 0.11, 0.17
10.0	101	3.4	0.14	29	0.57	0.03, 0.06, 0.09

different T dependences of J_c between YBCO and NCCO are expected, because the values of $\xi_c(0)$ and a_c are different between two materials as shown in Table 1.1 and Table 2.1. The values of ξ_c/a_c at $T = 0$ K for YBCO and NCCO is expressed by arrows in Fig.4.3 and ξ_c/a_c increases with increasing T.

Before discussing the temperature dependence of J_c , let us estimate the values of the critical current density at $\phi = 0°$ for YBCO and NCCO using eq.(4.5) and the calculated results of η_M. Tables 4.1 and 4.2 show the parameters used for estimating values of J_c at typical temperatures for YBCO and NCCO, respectively. These parameters were calculated from the experimental values at $T = 0$ K, $\xi_c(0) = 2.5$ Å, $\xi_{ab}(0) = 7.5$ Å and $B_c(0) = 1.0$ T for YBCO (from Table 2.1 and Refs.[11,12]), and $\xi_c(0) = 2.3$ Å, $\xi_{ab}(0) = 69$ Å and $B_c(0) = 0.2$ T for NCCO (from Table 2.1 and Ref.[13]). The values of $B_{irr}(0)$ were determined by the T dependence of $B_{irr}(T)$ in the high T region. Using these values of Tables 4.1 and 4.2 and η_M for three kinds of $\delta(= 0.2, 0.4, 0.6)$, the critical current densities for YBCO and NCCO at the typical temperature and field is obtained as shown in Tables 4.3 and 4.4.

For the YBCO thin film, the experimental values of J_c in the present thesis and our previous report[14] at $T = 77.3$ K are comparable to the estimated ones, however, the values at $T = 4.2$ K have one order of magnitude smaller than the

Table 4.3. Estimated values of J_c for YBCO for several values of $\delta = 0.2 - 0.6$.

T (K)	J_c (A/cm^2) at 0.5 T	J_c (A/cm^2) at 10 T
4.2	$5 - 15 \times 10^7$	$3.9 - 13 \times 10^7$
77.3	$7.3 - 22 \times 10^5$	$2 - 6 \times 10^5$

Table 4.4. Estimated values of J_c for NCCO for several values of $\delta = 0.2 - 0.6$.

T (K)	J_c (A/cm^2) at 0.5 T	J_c (A/cm^2) at 10 T
4.2	$4.3 - 13 \times 10^6$	$2.4 - 7.2 \times 10^6$
10.0	$1.2 - 3.6 \times 10^6$	$5.3 - 16 \times 10^5$

estimated ones. However, several groups reported that J_c for YBCO has the value of $\sim 5 \times 10^7$ A/cm^2 at $T = 4.2$ K[1,15] (see also Fig.2.1) which is similar to the estimated value.

As for NCCO thin films, the experimental value of J_c is smaller by a factor of $3 - 5$ than the value estimated above. The difference indicates that some other factors such as the flux creep effect and the small misalignment between B and the ab plane reduce the value of J_c . Nevertheless, the experimental one in this thesis is larger than the other group's values of J_c , *e.g.*, $J_c^M = 1.5 \times 10^4$ A/cm^2 at 4.2 K[16], $J_c = 2.0 \times 10^5$ A/cm^2 at 5.5 K[17] and $J_c = 7.3 \times 10^5$ A/cm^2 at 4.2 K[18].

The estimated values of J_c using the intrinsic pinning model largely depend on the value of δ. For example, the estimated value of J_c for $\delta = 0.8$ is larger by a factor of 4 than that for $\delta = 0.2$. Therefor, the difference between the experimental and the theoretical values of J_c within one order would not be surprising, so let us discuss T dependence of J_c by the intrinsic pinning model.

4.3.3 Temperature dependence of $J_c(B)$

Figure 4.4 shows double-logarithmic plots of J_c vs. $1-t^2$ for sample Y280A (YBCO) under various magnetic fields at $\phi = 0°$. A linearity of J_c in the figure is not good

except for the low temperature region. For conventional type II superconductors, in contrast to the results, a linear relation was obtained in double-logarithmic plots of J_c vs. $1-t^2$ or J_c vs. $1-t$, because the temperature dependence of J_c was expressed as $J_c(T) \propto F_p(T) \propto [B_{c2}(T)]^n$[6,19]. The nonliniality indicates that the pinning mechanism for HTSC is somewhat different from that for conventional materials. The calculated curves in the figure using the intrinsic pinning model of eq.(4.7) have a very similar characteristic feature, that is, rapid decrease of J_c at the high T region. The solid curves were calculated for $B = 1.0$ T and the curves 1, 2 and 3 correspond to the results for $\xi_c(0) = 2.0$, 2.5 and 3.0 Å ($\xi_c(0)/a_c = 0.17$, 0.21 and 0.26), respectively. The broken curve was calculated for $B = 12.0$ T with $\xi_c(0) = 2.5$ Å. Since the temperature dependence of η_M was scarcely dependent on δ, the calculation for temperature dependence in this chapter was performed only in the case of $\delta = 0.6$. For both calculations, a value of 150 T was used as $B_{irr}(0)$. The solid and the broken curves in Fig.4.1 also show calculated results for $B = 1.0$ T and 12.0 T in the case of $\xi_c(0) = 2.5$ Å ($\xi_c(0)/a_c = 0.21$). The measured $J_c(B,T)$'s agree with the calculated results at the low temperature and the high field region. However, a slight difference is seen at the high T and the low B region.

Figure 4.5 shows double-logarithmic plots of J_c vs. $1-t$ for the sample K4311 (NCCO) under various magnetic fields at $\phi = 0°$. The calculated results are shown by the solid curves for $B = 1.0$ T and by the broken curve for $B = 12.0$ T, respectively. The curves 1, 2 and 3 correspond to the results for $\xi_c(0) = 2.0$, 2.3 and 2.5 Å ($\xi_c(0)/a_c = 0.33$, 0.38 and 0.41), respectively. The curve 4 corresponds to the result for $\xi_c(0) = 2.3$ Å. The solid and the broken curves in Fig.4.2 also show calculated results for $B = 1.0$ T and 12.0 T in the case of $\xi_c(0) = 2.3$ Å ($\xi_c(0)/a_c = 0.38$). The parameter $B_{irr}(0) = 40$ T was used for the calculation. As shown in Figs.4.2 and 4.5, the measured $J_c(B,T)$'s agree with the calculated results at the low temperature and the high field region. However the measured J_c's at $B = 0.2$ T largely deviate from the calculated ones in the temperature region of

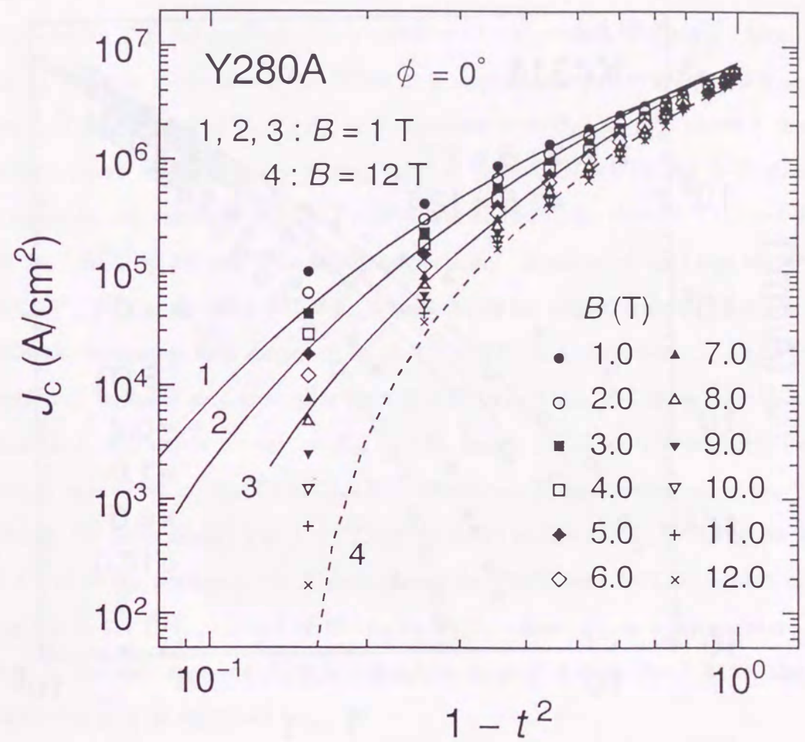

Fig. 4.4. Double-logarithmic plots of J_c vs. $1-t^2$ for sample Y280A (YBCO) under various magnetic fields at $\phi = 0°$. The solid curves were calculated for $B = 1.0$ T and the curves 1, 2 and 3 correspond to the results for $\xi_c(0) = 2.0$, 2.5 and 3.0 Å ($\xi_c(0)/a_c = 0.17$, 0.21 and 0.26), respectively. The broken curve was calculated for $B = 12.0$ T and the curve corresponds to the results for $\xi_c(0) = 2.5$ Å.

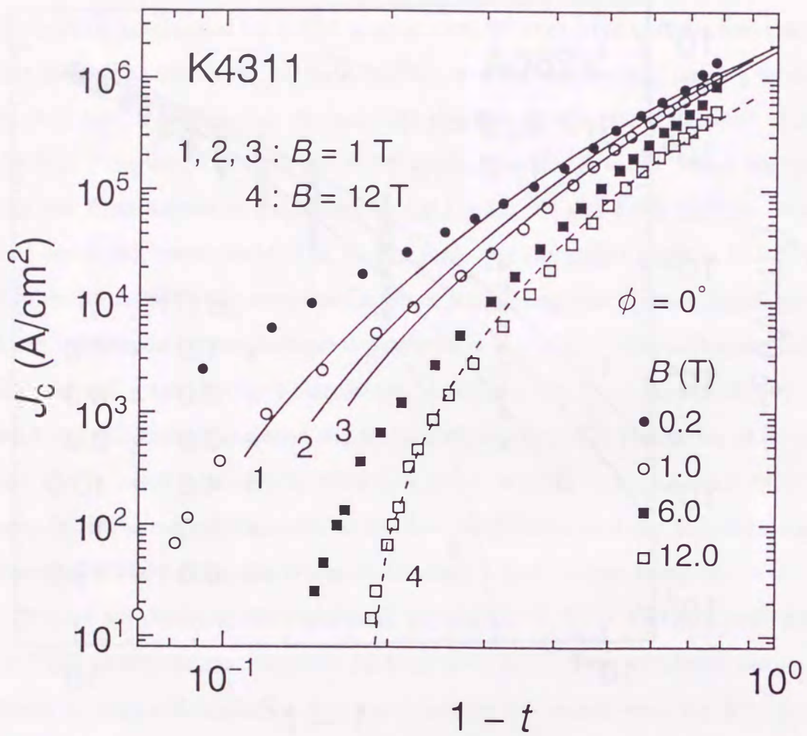

Fig. 4.5. Double-logarithmic plots of J_c vs. $1-t$ for sample K4311 (NCCO) under various magnetic fields at $\phi = 0°$. The solid curves were calculated for $B = 1.0$ T and the curves 1, 2 and 3 correspond to the results for $\xi_c(0) = 2.0$, 2.3 and 2.5 Å ($\xi_c(0)/a_c = 0.33$, 0.38 and 0.41), respectively. The broken curve was calculated for $B = 12.0$ T and the curve corresponds to the results for $\xi_c(0) = 2.3$ Å.

$t > 0.7$ and the disagreement may be related the other pinning effects except for intrinsic pinning. The existence of other pinning centers is supported by the flux pinning function under the magnetic field, which will be described in the following chapter.

As seen in Figs.4.4 and 4.5, $J_c(T)$ could not be expressed as a simple form of $J_c \propto (1-t)^n$ or $J_c \propto (1-t^2)^n$. When B is applied parallel to the basal plane, usually, B dependence of T_c, $T_c(B)$, or T dependence of B_{c2}, $B_{c2}(T)$, shows a characteristic curve with the sharp raising at $T = T_c$ and $B = 0$ in the B-T plane. For example, the values of $-[dB_{c2}(T)/dT]_{T_c}$ are known to be $10-24$ T/K and 9.3 T/K for YBCO[20,21] and NCCO[22], respectively. Because of the large slope of $-[dB_{c2}(T)/dT]_{T_c}$, the value of $T_c(B)$ is thought to be almost constant against B within the measured field range up to 12 T. In HTSC, a characteristic $B(T)$ line at which J_c becomes zero is smaller than $B_{c2}(T)$ line. Thus, the upper limit of the region at $J_c \neq 0$ exists below the $B_{c2}(T)$ line, and is called an irreversibility line, which is expressed as $B_{irr}(T)$ or $T_{irr}(B)$. Therefore, T dependence of J_c may be scaled by the form of $J_c(T) \propto [1-T/T_{irr}]^n$ or $J_c(T) \propto [1-(T/T_{irr})^2]^n$. Figures 4.6 and 4.7 show the scaling of the T dependence for YBCO and NCCO, respectively, using the factor T/T_{irr} instead of the factor T/T_c. Here, T_{irr} is a temperature at which J_c becomes zero and $J_c(0)$ is defined by J_c at $T = 0$ K. For YBCO, the T dependence of J_c is expressed as

$$J_c(T) = J_c(0)\left[1-\left(\frac{T}{T_{irr}}\right)^2\right]^{2.5} \tag{4.8}$$

under the magnetic field $B = 1.0-12.0$ T. As for NCCO, that is expressed as

$$J_c(T) = J_c(0)\left[1-\frac{T}{T_{irr}}\right]^3 \tag{4.9}$$

at $B = 1.0-12.0$ T. This universal scaling relation for each materials indicates that a common pinning mechanism such as the intrinsic pinning exists at $\phi = 0°$ in the measured region. However, J_c at $B = 0.2$ T deviates from the master lines

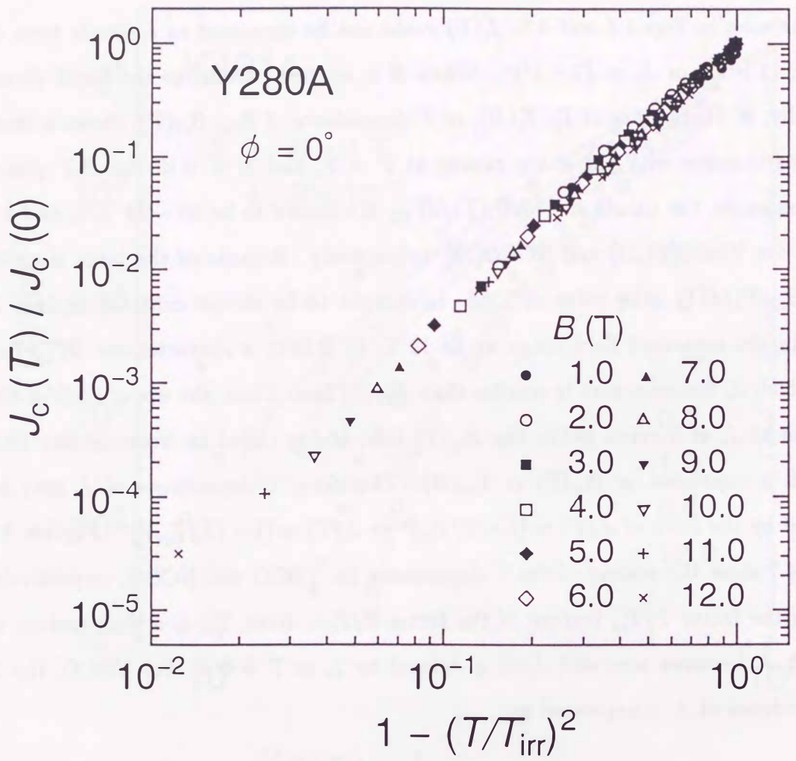

Fig. 4.6. Double-logarithmic plots of $J_c(T)/J_c(0)$ vs. $1-(T/T_{irr})^2$ for sample Y280A (YBCO) under various magnetic fields at $\phi = 0°$.

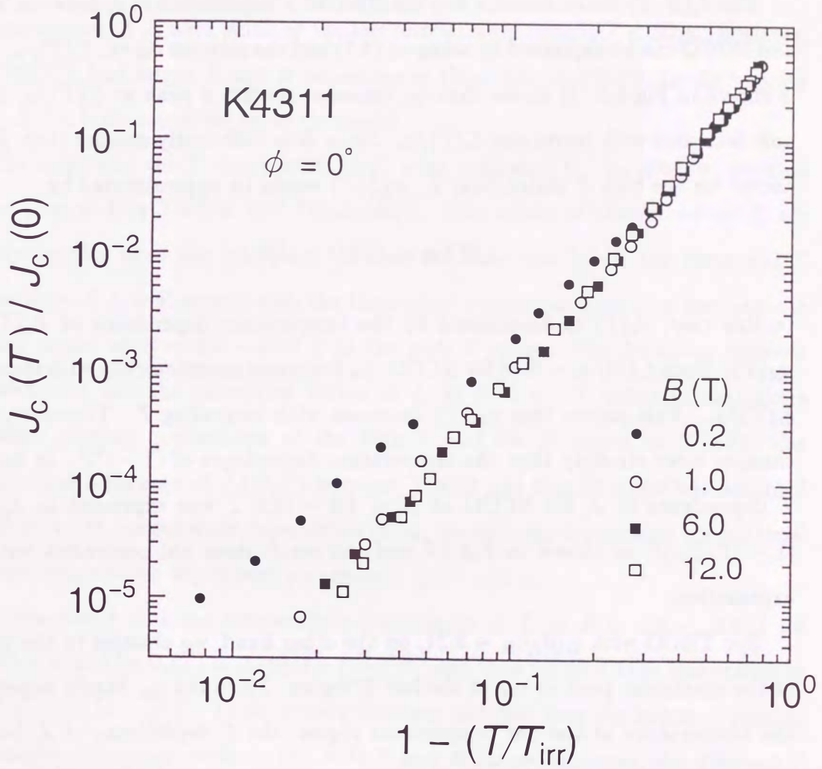

Fig. 4.7. Double-logarithmic plots of $J_c(T)/J_c(0)$ vs. $1-(T/T_{irr})$ for sample K4311 (NCCO) under various magnetic fields at $\phi = 0°$.

in the temperature region of $t > 0.7$, and the disagreement may be related to other pinning effects which will be discussed in the following chapter. Next, let us discuss the origin of the different T dependence between YBCO and NCCO.

The $J_c(B,T)$ characteristics and the different T dependence of J_c between YBCO and NCCO can be explained by using eq.(4.7) and the relation η_M vs. $\xi_c(T)/a_c$ which is shown in Fig.4.3. It shows that η_M increase, reaches a peak at $\xi_c(T)/a_c \simeq 0.28$ and decreases with increasing $\xi_c(T)/a_c$. Since B is sufficiently smaller than $B_{irr}(T)$ except for the high T region near T_c, eq.(4.7) would be approximated by

$$J_c(T) \propto \eta_M(T)\,(1-t^2)^2 \quad . \tag{4.10}$$

In this case, $J_c(T)$ is determined by the temperature dependence of $B_c(T)$ and $\eta_M(T)$. Since $\xi_c(0)/a_c \sim 0.38$ for NCCO, η_M decreases monotonically with increasing $\xi_c(T)/a_c$. This means that $\eta_M(T)$ decreases with increasing T. Therefore, $J_c(T)$ changes more strongly than the temperature dependence of $(1-t^2)^2$. In fact, the T dependence of J_c for NCCO at $B = 1.0 - 12.0$ T was expressed as $J_c(T) \propto [1-(T/T_{irr})]^3$ as shown in Fig.4.7 and the result does not contradict with this explanation.

For YBCO with $\xi_c(0)/a_c \sim 0.21$, on the other hand, η_M changes in the vicinity of the maximum peak of η_M at the low T region. Since the η_M hardly depends on the temperature at the low temperature region, the T dependence of J_c becomes weaker than the case of NCCO. However, η_M decreases gradually with increasing the temperature, so the decrease rate of $J_c(T)$ becomes slightly larger than the temperature dependence of $(1-t^2)^2$. Experimentally, T dependence of J_c for YBCO was obtained as $J_c(T) \propto [1-(T/T_{irr})^2]^{2.5}$ as shown in Fig.4.6. The factor $(T/T_{irr})^2$ indicates the weak temperature dependence at low temperatures as compared with the case of NCCO.

4.4 Summary

Transport critical current density $J_c(T, B)$ for YBCO and NCCO thin films at $B \parallel ab$ was investigated in a wide temperature range from 4.2 K to T_c. For YBCO, T and B dependences of J_c were small at the low temperature region, $T < 30$ K. However, J_c of NCCO had larger T and B dependences than that of YBCO. In the vicinity of T_c, J_c for both materials rapid decreased.

The value and the T dependence of J_c were estimated by the intrinsic pinning model proposed by Tachiki and Takahashi[5]. The values of the measured J_c are slightly smaller than the estimated values. On the other hand, the measured T dependence of J_c well agreed with the theoretical results calculated by the intrinsic pinning model at $B = 1.0 - 12.0$ T in the wide T range. The deviation between the measured and the calculated values of J_c at $B = 0.2$ T indicates that there are other pinning mechanisms at the high T and low B region in NCCO. The systematical difference of $J_c(B,T)$ between YBCO and NCCO could be explained by the different temperature dependence of η_M, because η_M depends on the material and the temperature dependent parameters, $\xi_c(T)$ and a_c.

It was found that the temperature dependence of J_c at $B = 1.0 - 12.0$ T for YBCO is scaled by $J_c(T) = J_c(0)\,[1-(\frac{T}{T_{irr}})^2]^{2.5}$ and that for NCCO is also scaled by $J_c(T) = J_c(0)\,[1-\frac{T}{T_{irr}}]^3$. These scaling relations indicate that the intrinsic pinning mechanism commonly works in the wide T and B ranges, however, the different T dependence of J_c would be determined by the material dependent parameters.

References

[1] B. Roas, L. Schultz and G. Saemann-Ischenko, *Phys. Rev. Lett.* **64** (1990) 479.

[2] Y. Iye, T. Terashima and Y. Bando, *Physica C* **184** (1991) 362.

[3] M. Tachiki and S. Takahashi, *Solid State Commun.* **72** (1989) 1083.

[4] S. Awaji, K. Watanabe, N. Kobayashi, H. Yamane and T. Hirai, *Jpn. J. Appl. Phys.* **31** (1992) L1532.

[5] M. Tachiki and S. Takahashi, *Solid State Commun.* **70** (1989) 291.

[6] D. Dew-Hughes, *Philos. Mag.* **30** (1974) 293.

[7] E. J. Kramer, *J. Appl. Phys.* **44** (1973) 1360.

[8] K. E. Gray, R. T. Kampwirth, J. M. Murduck and D. W. Capone II, *Physica C* **152** (1988) 445.

[9] S. Kubo, Y. Enomoto and T. Iwata, *Adv. Supercond. III, Proc. 3rd Int. Symp. Superconductivity, Sendai, 1990* (Springer-Verlag, Tokyo, 1991) p.559.

[10] T. Nishizaki, T. Aomine, I. Fujii, K. Yamamoto, S. Yoshii, T. Terashima and Y. Bando, *Physica C* **181** (1991) 223.

[11] M. B. Salamon, and J. Bardeen, *Phys. Rev. Lett.* **59** (1987) 2615.

[12] U. Welp, W. K. Kwok, G. W. Crabtree, K. G. Vandervoort and J. Z. Liu, *Phys. Rev. Lett.* **62** (1989) 1908.

[13] D. H. Wu, J. Mao, S. N. Mao, J. L. Peng, X. X. Xi, T. Venkatesan, R. L. Greene and S. M. Anlage, *Phys. Rev. Lett.* **70** (1993) 85.

[14] T. Nishizaki, F. Ichikawa, T. Fukami, T. Aomine, T. Terashima and Y. Bando, *Physica C* **204** (1993) 305.

[15] G. Koren, A. Gupta and T. R. McGuire, *Appl. Phys. Lett.* **54** (1989) 1054.

[16] J. Fontcuberta, S. Piñol, X. Obradors, F. Lera and C. Rillo, *Cryogenics* **30** (1990) 656.

[17] A. Gupta, G. Koren, C. C. Tsuei, A. Segmüller and T. R. McGuire, *Appl. Phys. Lett.* **55** (1989) 1795.

[18] S. Hatta, S. Hayashi, H. Adachi and K. Wasa, *Jpn. J. Appl. Phys.* **28** (1989) L1201.

[19] W. A. Fietz and W. W. Webb, *Phys. Rev.* **178** (1969) 657.

[20] U. Welp, W. K. Kwok, G. W. Crabtree, K. G. Vandervoot and J. Z. Liu, *Phys. Rev. Lett.* **62** (1989) 1908.

[21] J. J. M. France, J. N. Li and K. Kadowaki, *High Temperature Superconductivity - Vol.24, Proc. European Conference on High-T_c Thin Films and Single Crystals, Poland, 1989* (World Scientific, Singapore, 1990) p.72.

[22] M. Suzuki and M. Hikita, *Phys. Rev. B* **41** (1990) 9566.